

INVESTIGATING HYDROTHERMAL AND RADIATION EFFECTS ON
NITROGEN HETEROCYCLES RELEVANT TO METEORITE PARENT BODIES

by

Phillip G. Hammer

A thesis

submitted in partial fulfillment

of the requirements for the degree of

Master of Science in Chemistry

Boise State University

August 2017

© 2017

Phillip G. Hammer

ALL RIGHTS RESERVED

BOISE STATE UNIVERSITY GRADUATE COLLEGE

DEFENSE COMMITTEE AND FINAL READING APPROVALS

of the thesis submitted by

Phillip G. Hammer

Thesis Title: Investigating Hydrothermal and Radiation Effects on Nitrogen Heterocycles Relevant to Meteorite Parent Bodies

Date of Final Oral Examination: 12 June 2017

The following individuals read and discussed the thesis submitted by student Phillip G. Hammer, and they evaluated his presentation and response to questions during the final oral examination. They found that the student passed the final oral examination.

Michael P. Callahan, Ph.D. Chair, Supervisory Committee

Dale D. Russell, Ph.D. Member, Supervisory Committee

Don Warner, Ph.D. Member, Supervisory Committee

The final reading approval of the thesis was granted by Michael P. Callahan, Ph.D., Chair of the Supervisory Committee. The thesis was approved by the Graduate College.

DEDICATION

To my family and friends, loved ones, who without their support both past and present I would not have made it this far.

ACKNOWLEDGEMENTS

I would like to thank the NASA Earth and Space Science Fellowship (NESSF) for supporting this research and my graduate studies. I would also like to thank the ELSI (Earth-Life Science Institute) Origins Network for supporting this research. I would especially like to thank Dr. Henderson (Jim) Cleaves who acted as my guide and colleague while conducting research at the Tokyo Institute of Technology in Japan. I consider him a friend now. In addition, I want to thank Ruiqin Yi, Mayuko Nakagawa, and Kyoko Akiyama for their hard work and their help guiding me through working in a foreign laboratory. Thank you to Dr. Aaron Burton and Dr. Darren Locke at NASA Johnson Space Center for analyzing NH_4CN polymers by TMAH GC-MS and providing the data for me to analyze. I would like to thank Dr. Karen Smith for reading and editing my thesis. Finally, I would like to thank the faculty and staff in the Department of Chemistry and Biochemistry including those on my thesis committee who helped me throughout graduate school. I'm proud to say Boise State University is my alma mater for both my B.S. and M.S. degrees in Chemistry. Prof. Callahan...you know what you did. I blame all this - the research, the travel, the conferences, continuing to pursue a doctorate, and this dissertation ON YOU!!!

ABSTRACT

Organic compounds in meteorites were likely transformed by a variety of processes on the asteroid parent body including aqueous, thermal, and radiolytic alteration. Previous studies have identified a suite of purine nitrogen heterocycles in carbonaceous chondrites (a class of meteorites) and determined that their likely origin was due to cyanide chemistry. The thesis research described here consisted of two parts: investigating thermal effects on aqueous ammonium cyanide reactions and the production/survivability of organics (Chapter 2) and investigating gamma radiation effects on purine nitrogen heterocycles to understand how prolonged radiation exposure influenced the distribution and abundance of nitrogen heterocycles measured in meteorites today (Chapter 3).

A temperature study of 1 M ammonium cyanide was conducted from room temperature to 200 °C (temperatures similar to the aqueous alteration of some carbonaceous chondrites) using a high-pressure reaction vessel. The resulting liquid supernatant and water insoluble cyanide (hetero)polymer were isolated and analyzed by attenuated total reflectance Fourier transform infrared spectroscopy and thermochemolysis gas chromatography-mass spectrometry using tetramethylammonium hydroxide or high-performance liquid chromatography with UV detection (HPLC-UV). A strong correlation was observed between thermochemolysis products of cyanide polymers and the initial reaction temperature - production of aromatic compounds increases and nitrogen containing compounds decrease with respect to increasing reaction temperature. The data presented in this thesis suggests that the polymer may be a less efficient source of nitrogen

heterocycles when produced at high temperatures. HPLC-UV analysis showed that the supernatant of heated NH_4CN reactions is a complex mixture containing many unknown UV-absorbing chromophores. In addition, multiple nitrogen heterocycles were *tentatively* identified in the supernatant of heated NH_4CN reactions including the high temperature 200 °C reactions.

Finally, HPLC was used to determine decomposition of seven purine nitrogen heterocycles exposed to gamma radiation from a cobalt-60 source in an effort to extrapolate abundances during the early formation of the Solar System. Generally speaking, purine nitrogen heterocycles in the solid state are very stable to high doses of γ -radiation; however, guanine experienced a 53% decomposition over the course of ~1 MGy of radiation dose. The radiolysis study correlates to similar conditions in asteroids after their initial aqueous alteration period (*i.e.* dry alteration) and suggests that meteorite abundances for some compounds (such as adenine) may have remained relatively unchanged over time, but other compounds (like guanine) may have had “original” abundances greater than those currently observed in carbonaceous chondrites.

TABLE OF CONTENTS

DEDICATION	iv
ACKNOWLEDGEMENTS	v
ABSTRACT	vi
LIST OF TABLES	x
LIST OF FIGURES	xi
LIST OF ABBREVIATIONS	xiv
CHAPTER ONE: INTRODUCTION AND BACKGROUND	1
Organic Compounds and Cyanide as a Precursor	1
Extraterrestrial Materials: Asteroids and Meteorites	6
Secondary Processing in Extraterrestrial Materials	8
Temperature Studies of Cyanide Reactions	9
Radiation Studies of Nitrogen heterocycles	11
CHAPTER TWO: HYDROTHERMAL CYANIDE REACTIONS	12
Introduction	12
Experimental Methods	12
Materials	12
Sample Preparation	13
Instrumental Methods	14
Results and Discussion	22

Initial Observations of Cyanide Reactions	22
Infrared Spectroscopy of the Cyanide Supernatant and Polymer	23
Thermochemolysis of Cyanide Polymer Using TMAH GC-MS.....	28
Qualitative Identification of Nitrogen heterocycles Using HPLC	36
Conclusion	45
CHAPTER THREE: GAMMA RADIOLYSIS OF NITROGEN HETEROCYCLES	48
Introduction.....	48
Experimental Methods	49
Materials	49
Sample Preparation	50
High Performance Liquid Chromatography	52
Results and Discussion	54
Conclusion	68
REFERENCES	70
APPENDIX A.....	75

LIST OF TABLES

Table 2.1.	Nominal mass data and empirical formulas for nitrogen heterocycle thermochemolysis products	20
Table 2.2.	Polymer mass and (% wt/wt) of each cyanide reaction	23
Table 2.3.	Compounds identified in room temperature polymer samples as determined by TMAH-GC-MS	31
Table 2.3 Continued.	Compounds identified in room temperature polymer samples as determined by TMAH-GC-MS	32
Table 2.4.	HPLC-UV retention times of nitrogen heterocycles.....	38
Table 2.5.	HPLC-UV determination of nitrogen heterocycles present in the reaction matrix	45
Table 3.1.	Total dose versus time data.....	51
Table 3.2.	Dose rate versus time data	51
Table 3.3.	Percent recovery of γ -irradiated nitrogen heterocycles in the total dose study.....	64
Table 3.4.	Percent recovery of γ -irradiated purines in the dose rate study	67
Table A.1.	Compound names and structures for the products identified in the thermochemolysis TMAH-GC-MS analysis.....	76

LIST OF FIGURES

Figure 1.1.	Time lapse photos of a room temperature aqueous ammonium cyanide reaction.....	2
Figure 1.2.	Generally accepted cyanide reaction pathway to produce adenine	4
Figure 1.3.	Example of a ribonucleotide	6
Figure 1.4.	Purine nitrogen heterocycles specifically sought in this study	7
Figure 2.1.	General scheme for reaction preparation, work-up and analysis	15
Figure 2.2.	Perkin Elmer spectrum 100 FTIR Spectrometer equipped with U-ATR accessory (with components labeled)	16
Figure 2.3.	Thermochemolysis GC-MS (with components labeled) used for the analysis of cyanide polymer. Photo courtesy of Dr. Darren Locke and Dr. Aaron Burton of the NASA Johnson Space Center	18
Figure 2.4.	Thermochemolysis sample unit	18
Figure 2.5.	HPLC-UV instrument (with components labeled) used for the analysis of supernatant portions of heated ammonium cyanide reactions	22
Figure 2.6.	IR spectra of supernatant (orange) and polymer (black) obtained from a 6-month, room temperature NH_4CN reaction	24
Figure 2.7.	IR spectra of supernatant from NH_4CN reaction heated at different temperatures for 72 hours	25
Figure 2.8.	IR spectra of polymer obtained from NH_4CN reactions heated at different temperatures for 72 hours	26
Figure 2.9.	Close-up of IR spectra of polymer obtained from NH_4CN reactions heated at different temperatures for 72 hours.....	28
Figure 2.10.	GC-MS total ion chromatogram with thermochemolysis products of room temperature cyanide polymer labeled	29

Figure 2.11.	Total ion chromatograms of polymer samples synthesized at different reaction temperatures for 72 h that have been measured by thermochemolysis GC-MS.....	30
Figure 2.12.	Relative peak area versus temperature plots of thermochemolysis products of cyanide polymer	33
Figure 2.13.	Relative peak area versus temperature plots of thermochemolysis products of cyanide polymer	34
Figure 2.14.	Relative peak area versus temperature plots of thermochemolysis products of cyanide polymer	34
Figure 2.15.	Comparison of extracted ion chromatograms of adenine (nucleobase) and benzene (aromatic) production in thermochemolysis products of NH ₄ CN polymers.....	35
Figure 2.16.	HPLC-UV chromatograms of four different mixtures of nitrogen heterocycle reference standards in 0.1 M NH ₄ OH.....	37
Figure 2.17.	UV chromatograms of the supernatant isolated from NH ₄ CN reactions heated at different temperatures for 3 hours	40
Figure 2.18.	UV chromatograms of the supernatant isolated from NH ₄ CN reactions heated at different temperatures for 24 hours	40
Figure 2.19.	UV chromatograms of the supernatant isolated from NH ₄ CN reactions heated at different temperatures for 72 hours	41
Figure 2.20.	UV chromatograms of the supernatant isolated from NH ₄ CN reactions heated at 50 °C for different times	41
Figure 2.21.	UV chromatograms of the supernatant isolated from NH ₄ CN reactions heated at 150 °C for different times	42
Figure 2.22.	UV chromatograms of the supernatant isolated from NH ₄ CN reactions heated at 200 °C for different times	42
Figure 3.1.	Radiolysis sample placement at the ⁶⁰ Co source. Gamma Radiation Facility, Tokyo Institute of Technology in Japan.	53
Figure 3.2.	Purine nitrogen heterocycles investigated in the γ-irradiation studies.....	54
Figure 3.3.	Purine calibration curve.	55
Figure 3.4.	Adenine calibration curve.	56

Figure 3.5.	Guanine calibration curve.	56
Figure 3.6.	Hypoxanthine calibration curve.	57
Figure 3.7.	Xanthine calibration curve.	57
Figure 3.8.	2,6-diaminopurine calibration curve.	58
Figure 3.9.	6,8-diaminopurine calibration curve.	58
Figure 3.10.	Total dose decay curve for purine.	60
Figure 3.11.	Total dose decay curve for adenine	61
Figure 3.12.	Total dose decay curve for hypoxanthine	62
Figure 3.13.	Total dose decay curve for guanine	62
Figure 3.14.	Total dose decay curve for xanthine	63
Figure 3.15.	Total dose decay curve for 2,6-diaminopurine	63
Figure 3.16.	Total dose decay curve for 6,8-diaminopurine	64
Figure 3.17.	Amine substitution effects on the γ -radiolysis of purine heterocycles	65
Figure 3.18.	De-amination effect on the γ -radiolysis of purine heterocycles	66
Figure 3.19.	Dose rate analysis of purine nucleobases.	68

LIST OF ABBREVIATIONS

AICA	aminoimidazole carboxamide
AICN	aminoimidazole carbonitrile
ATR-FTIR	attenuated total reflectance Fourier transform infrared spectroscopy (or spectrometer)
BSU	Boise State University
CN^-	cyanide anion
DAMN	diaminomaleonitrile
DNA	deoxyribonucleic acid
ETM	extraterrestrial material
GC-MS	gas chromatography-mass spectrometry (or spectrometer)
Gy/MGy	Gray / MegaGray
HCN	hydrogen cyanide
HPLC	high performance liquid chromatography (or chromatograph)
IOM	insoluble organic material
JSC	Johnson Space Center
KCN	potassium cyanide
keV/MeV	kiloelectronvolt / megaelectronvolt
LC-MS	liquid chromatography-mass spectrometry (or spectrometer)
NASA	National Aeronautics and Space Administration
NH_4Cl	ammonium chloride

NH ₄ CN	ammonium cyanide
NH ₄ OH	ammonium hydroxide
NIST/EPA/NIH	National Institute of Standards and Technology / Environmental Protection Agency / National Institutes of Health
RNA	ribonucleic acid
TMAH	tetramethylammonium hydroxide

CHAPTER ONE: INTRODUCTION AND BACKGROUND

Consider the plethora of organic compounds found in meteorites and how these complex materials formed. What were the starting materials used to create this dynamic array of organics? What conditions were experienced by the parent body asteroid during their 4.568 billion years of aging?¹ Finally, how stable are these chemicals in a harsh cosmic environment? Attempting to elucidate answers to these questions is the objective of this thesis.

Organic Compounds and Cyanide as a Precursor

Using millimeter-wave line emissions of cyanide anion (CN^-) and hydrogen cyanide (HCN) molecules, these compounds have been detected in distant galaxies, planetary nebula, circumstellar disks, and interstellar gas clouds and are notably associated with star-forming regions of the cosmos, which are all regions of space with the appropriate energies to form cyanide.²⁻⁵ Therefore, cyanide is found in a variety of locations throughout the cosmos and is considered ubiquitous.

Cyanide is a highly reactive molecule. Successive interaction of cyanide with other cyanide molecules will produce an increasingly complex organic material in a monomer addition process termed self-polymerization.⁶⁻⁸ This process is often initiated by the presence of ammonia, which is also cosmically abundant.^{9, 10} The chemical complexity may be further altered by the presence of other compounds, any side products, the presence of water, and the degree of heating.

In the laboratory, ammonium cyanide (NH_4CN) reactions are often carried out under ambient conditions (*i.e.* atmospheric pressure and room temperature). After several hours, a slight yellow color develops in aqueous solutions of NH_4CN . After a few days, a black precipitate forms, and over the course of weeks to months the reaction becomes increasingly dark with a significant amount of precipitate build-up. **Figure 1.1** provides a visual of this process for a room temperature ammonium cyanide reaction over the course of two weeks. **Figure 1.1** also shows an ammonium cyanide reaction that was heated at 90°C for 2 minutes (shown within the yellow box), and demonstrates that these reactions can be accelerated by heat as evidenced by the rapid color change. Once the reaction has progressed sufficiently, it is centrifuged or filtered to remove the black precipitate from the orange-colored supernatant providing two analyzable fractions.

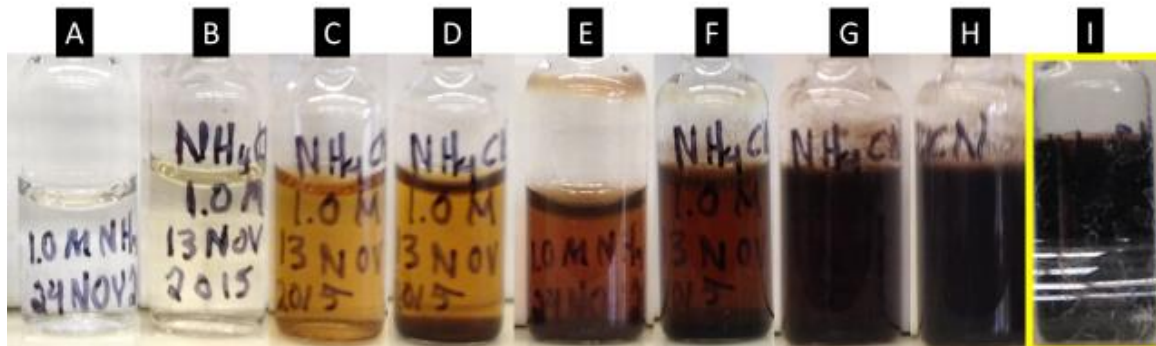


Figure 1.1. Time lapse photos of a room temperature aqueous ammonium cyanide reaction. (A) Initially a clear colorless solution of NH_4CN . (B) Four hours after initiation, the reaction has a light yellow color. (C) After one day, the reaction has turned light brown and a precipitate begins to form. (D) 48 hours. (E) 72 hours. (F) 120 hours. (G) 216 hours. (H) 336 hours. (I) Freshly prepared NH_4CN solution heated at 90°C for 2 minutes.

Cyanide can be made in several ways. For example, the Miller-Urey experiment used an electric discharge inside a methane, ammonia, hydrogen, and water (vapor) atmosphere in order to study the formation of more complex organic compounds under

conditions meant to simulate an early Earth with a reducing atmosphere.¹¹⁻¹³ In subsequent studies, cyanide was found to be produced and played an important role as an essential reaction intermediate, for example, in the synthesis of amino acids.^{14, 15} This was a startling discovery to the scientific community as never before had amino acids been produced in an abiotic synthesis.

Around this time, studies involving aqueous ammonium cyanide reactions also appeared. Initial investigations of the supernatant were performed by Juan Oró in the early 1960s, which revealed the presence of adenine.¹⁶ Adenine is a bicyclic (purine) nitrogen heterocycle common to biological processes and can also be considered a pentamer of cyanide.¹⁷ Further study of ammonium cyanide reactions revealed a complex series of reaction steps. The reaction scheme in **Figure 1.2** displays the generally accepted reaction pathway for the production of adenine as well as hypoxanthine.^{18, 19} In this reaction scheme, cyanide is shown to react with two additional cyanide molecules to produce a trimer called aminomalononitrile. The trimer can then react with another cyanide molecule to produce the tetramer, diaminomaleonitrile (DAMN), which can undergo isomerization and cyclization to form a five membered (imidazole) nitrogen heterocycle named amino imidazole carbonitrile (AICN). AICN will react with another cyanide molecule to produce a biologically relevant nitrogen heterocycle (nucleobase), adenine. Additionally, the nitrile group on AICN can hydrolyze to produce amino imidazole carboxamide (AICA) which can react with cyanide, releasing ammonia, and produce hypoxanthine. Likewise the deamination of adenine (loss of amine group and replacement with a carbonyl group) will also produce hypoxanthine. Research conducted since Oró's discovery has revealed the presence of several more compounds including six membered ring (pyrimidine) nitrogen

heterocycles. For example, a study performed by Miyakawa *et al.* froze aqueous ammonium cyanide solutions at $-78\text{ }^{\circ}\text{C}$ for 27 years and analyzed the supernatant and polymer under non-hydrolyzed, acid hydrolyzed, and alkaline hydrolyzed extraction conditions to reveal the presence of 11 different nitrogen heterocycles.²⁰

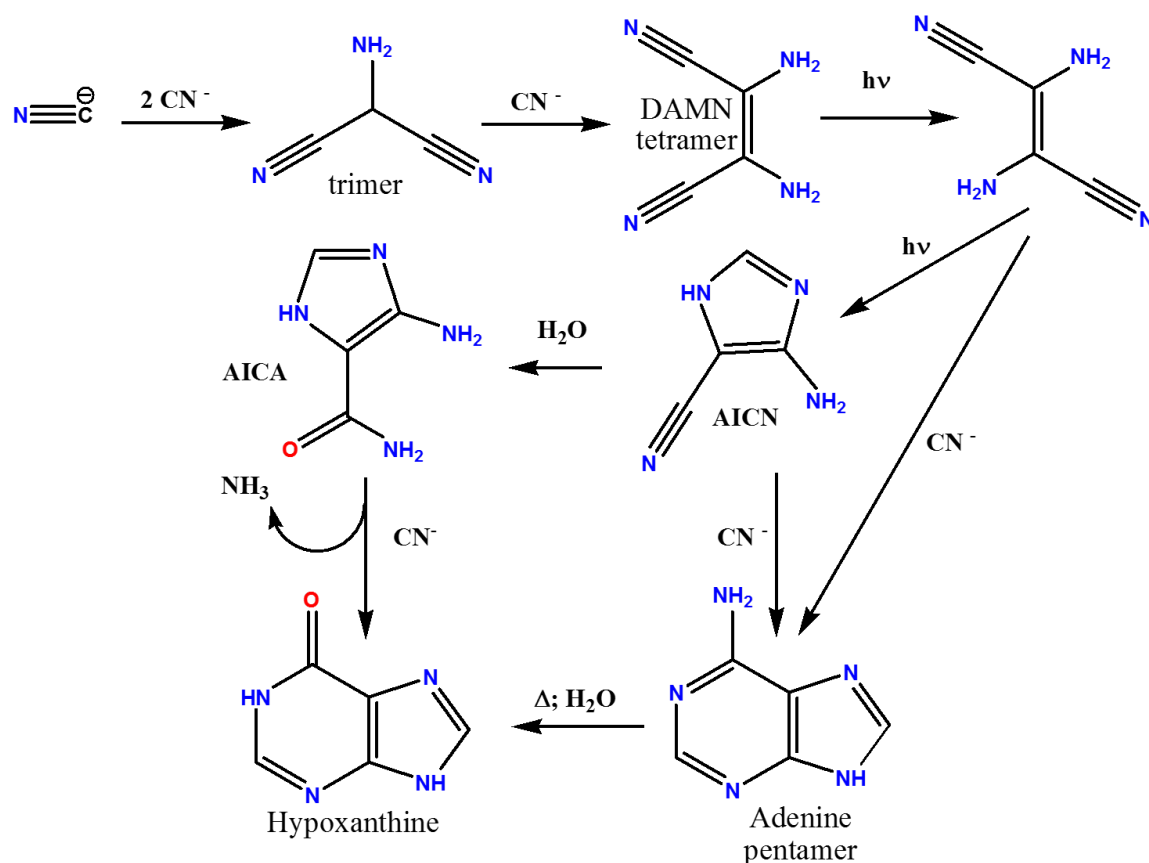
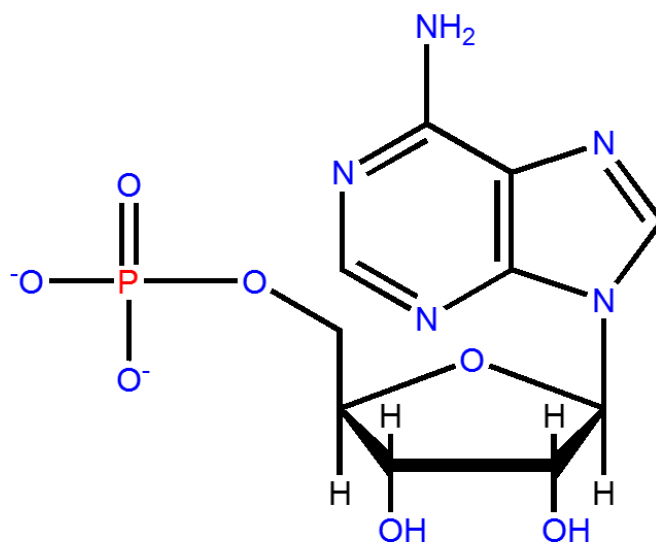


Figure 1.2. Generally accepted cyanide reaction pathway to produce adenine. The trimer is aminomalononitrile. The tetramer is diaminomaleonitrile which will cyclize to form aminoimidazole carbonitrile (AICN). AICN can hydrolyze to form aminoimidazole carboxamide (AICA) or react with cyanide to produce adenine. AICA will react with cyanide to produce hypoxanthine. Deamination of adenine will also produce hypoxanthine.

Thus far, the discussion has focused primarily on the analysis of the supernatant. The cyanide polymer (precipitate), however, is a different story. The precipitate is a complex organic material whose structure is not well understood. Several types of structures have been proposed to explain much of the data gathered for this recalcitrant

material.^{21, 22} One structure of cyanide polymer proposed by Minard and Matthews is composed of a polynucleobase chain structure, wherein synthesized nitrogen heterocycles (as “monomers”) are thought to be incorporated.²³ This type of proposed structure provides an explanation for the release of nitrogen heterocycles from the cyanide polymer upon acid hydrolysis.²³ This example also provides credence to a widely accepted terminology referring to the cyanide precipitate as a polymer.

From an origin of life perspective, the most important nitrogen heterocyclic molecules may be the canonical nucleobases: adenine, guanine, thymine, cytosine, and uracil. A nucleobase can be functionalized with a ribofuranose sugar group to yield a nucleoside. Further modification with a phosphate group yields a nucleotide, which is the monomer unit of DNA/RNA that are essential for all known life on Earth. Shown in **Figure 1.3** is adenosine monophosphate, a ribonucleotide in RNA. Studies by Callahan *et al.* identified a suite of seven extraterrestrial nitrogen heterocycles including adenine and guanine in carbonaceous chondrites (meteorites), as shown in **Figure 1.4**, and found that these same nitrogen heterocycles were also detected in aqueous ammonium cyanide reactions.²⁴



Adenosine monophosphate

Figure 1.3. Example of a ribonucleotide. Nucleotides are monomers found in the biological polymers ribonucleic acid (RNA) and deoxyribonucleic acid (DNA). These compounds are essential to all known life on Earth.

Extraterrestrial Materials: Asteroids and Meteorites

Asteroids make up a significant portion of the extraterrestrial materials (ETM) in our Solar System and these ETM are primarily confined to the Asteroid Belt, but there are Kuiper Belt objects out past Neptune and Pluto.²⁵⁻²⁷ The Asteroid Belt is located between Mars and Jupiter, approximately 386 million km from Earth.²⁸ It is theorized that Jupiter had a very strong effect on the current form of our Solar System and that Jupiter's strong gravity caused tidal forces significant enough to prevent the asteroid belt from fully accreting into a planet. The result is a region of space populated with primitive objects containing materials which have not been altered by atmospheric or geologic processes. The facts that these materials are as old as the Solar System and have not been perturbed to a significant extent makes asteroids a valuable material to the scientific community.

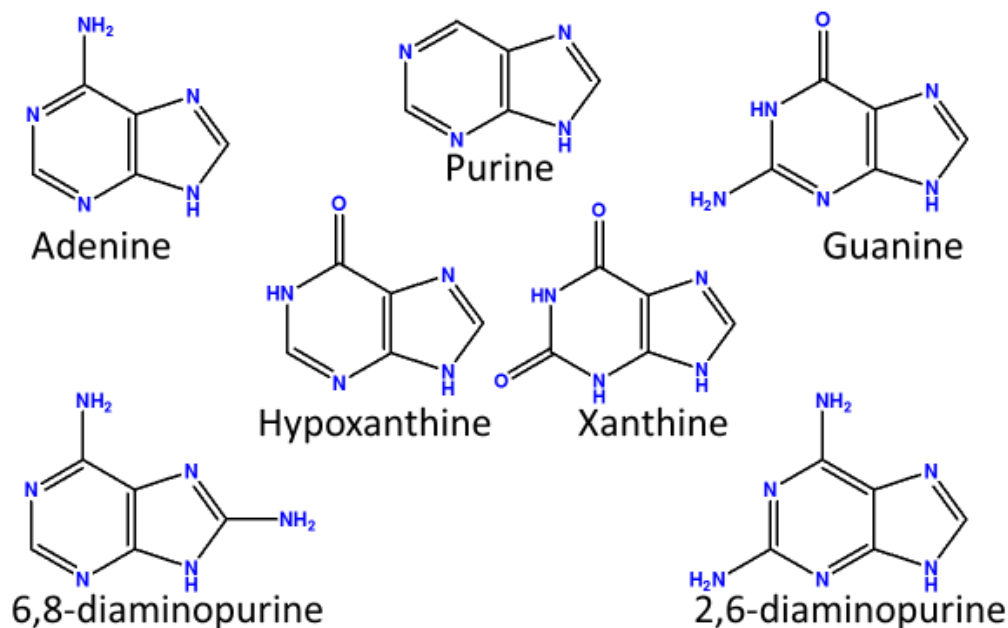


Figure 1.4. Purine nitrogen heterocycles specifically sought in this study. All of these compounds have been identified in formic acid extracts of meteorites and are produced in room temperature aqueous ammonium cyanide reactions.

According to the Nice model, the gravity of Jupiter has absorbed, skewed, and abducted many small bodies in the Solar System.²⁹ It is this effect of orbital skewing in solar system bodies that careens these masses onto courses bound for other bodies. This causes asteroids to collide with other asteroids, fragment, and send smaller materials (meteoroids) on very different paths. Often enough, these small bodies make their way to other planetary bodies. Currently, it is estimated that Earth receives between 10^5 to 10^6 kg of ETM a day.^{30,31} Taking into account a gradual diminishing of cosmic material with time and the craters observed on other planets and satellites, turning back the clock a few billion years suggests a much higher influx of ETM to an early Earth (and other planetary bodies in the Solar System) and is referred to as the Late Heavy Bombardment.³² This provided appreciable amounts of material not present as a result of accretion and can be accredited to “Jupiter Skewing” of ETM. This may be considered a reasonable explanation as to why

the Earth developed oceans via water-containing asteroids and comets.³³ This may have been accompanied by an influx of organic materials including simple (cyanide) and complex molecular compounds (nitrogen heterocycles) that may have influenced prebiotic chemistry.³⁴ These compounds have been identified in the analysis of meteorites.^{24, 35} Specifically, the nitrogen heterocycles and nucleobases found in meteorites are the same suite as those found in cyanide chemistry.²⁴ Acknowledging that cyanide is a ubiquitous compound and the correlation between these two data sets, scientists can reasonably surmise that many of the organics present in meteorites owe their formation to cyanide chemistry.

Secondary Processing in Extraterrestrial Materials

Secondary processing refers to the wide range of conditions that extraterrestrial materials have experienced throughout their existence. Contrary to initial assumption, our Sun is not the principle source of energy driving the thermal processing of organic matter in asteroids. Heat energy used to drive aqueous alteration and/or thermal metamorphism is considered to come from several sources all of which potentially have the same effects in processing the mineral and organic components inside asteroids.³⁶

Shock metamorphism, thermal metamorphism, and aqueous alteration all affect mineralogical and chemical processing. Thermal metamorphism is a broad range of conditions involving the heat produced during shock wave propagation, gravitational compression, and decay of radioactive elements. Each of these can be affected by the presence of water, further affecting mineral phases and chemical composition. This makes classification even more complex.³⁷ Over time, the radioactive decay of elements in these materials have released energy in the form of heat. This heat can be sufficient to melt water

ice present and cause aqueous chemical alteration.³⁸ This process has been shown in studies of mineral morphologies contained within the chondrules of meteorites.³⁹ Continued and more pronounced heating can both evaporate this water and cause more significant chemical alterations called thermal metamorphosis.³⁷

This thesis research is focused on the chemical aspects of aqueous and thermal alteration in secondary processing and how these alter chemical reactions, nitrogen heterocycle formation, and the distribution of bio-organics in parent asteroids. A key note is that the line between aqueous and thermal alteration is blurred and not distinct. The effect of relative nucleobase abundances with respect to other nitrogen heterocycle formation as well as other bio-relevant compounds shines light on what was available as feedstock during the early formation of life on Earth and possibly elsewhere (either in the Solar System or more distant regions of the universe). The research presented here is focused on the thermal effects on aqueous cyanide chemistry, specifically nucleobase production and how temperature influences the distribution and survivability of these compounds. Additionally, radioactive decay is necessary to this research as the high energy gamma rays emitted during the decay process are capable of inducing additional chemical alteration. In this study, gamma radiation from a cobalt-60 (⁶⁰Co) source was used to determine decay/survivability of seven purine nitrogen heterocycles in the solid state.

Temperature Studies of Cyanide Reactions

In the discovery of adenine as a product of cyanide reactions, Oró refluxed aqueous ammonium cyanide solutions.¹⁶ Studies by Miyakawa *et al.* conducted reactions at -80 and -20 °C.²⁰ Borquez *et al.* conducted studies at 60, 80, and 100 °C and compared this data to that of Miyakawa.⁴ One of the notable conclusions was that the production of adenine does

not have a significant dependence on temperature, as abundances increased slightly from 0.04% at -80 °C to 0.12 % at 100 °C. The question arises - How do the relative abundances of all the nitrogen heterocycles in these reactions change with increasing temperature? The previous studies focused on adenine, guanine, and 2,6-diaminopurine only. Thermal studies performed on cyanide polymer (prepared from alkali metal-cyanide salts) showed the formation of cyanide, isocyanic and cyanic acid as well as formamide. This same study showed a dependence on the atmosphere under which the polymer was heated/degraded and in the absence of oxygen a significant portion of the carbonized polymer remained at 1000 °C.⁴⁰ Although, it is unknown whether nitrogen heterocycles can still be released from the cyanide polymer after extensive high temperature heating. The meteorites which have been analyzed for nitrogen heterocycles belong to the lower temperature, aqueously altered groupings of ETM. We believe that a thermal study of cyanide reactions will be relevant to the distribution of biologically relevant nucleobases and nitrogen heterocycles throughout an array of ETM that have experienced a broader range of temperatures.

So, it is reasonable to ask the question “How does thermal alteration affect the production of nucleobases/nitrogen heterocycles in cyanide chemistry?” Answering this question has been no trivial pursuit. This involved heating cyanide reactions to various temperatures in specialized high-pressure reaction vessels. To show thermal effects on cyanide chemistry, the production of 13 different nitrogen heterocycles was tracked at differing temperatures ranging from 20 °C (room temperature) to 200 °C in 50 °C increments. The duration of these reactions ranged from three hours to three days at the respective temperatures.

Radiation Studies of Nitrogen heterocycles

Primitive asteroids contained a variety of radionuclides including ^{26}Al , ^{238}U , ^{232}Th and ^{40}K .^{41, 42} The last three have long half-lives and undergo a series of decay events emitting high-energy particles and gamma rays of sufficient energy to break covalent bonds (0.1 to >100 keV). Thus, radioactive decay can induce the breakdown and complexification of organic compounds. Radiolysis is of fundamental interest for origin of life studies as it may contribute to the alteration of astromaterials before their delivery to the surface of primitive planets.

This study also investigated the stability/survivability of nitrogen heterocycles exposed to gamma radiation. Nitrogen heterocycle reference compounds (the same nitrogen heterocycles searched for in the thermal study) were exposed to different doses of gamma radiation in the solid state. Additionally, canonical nucleobases were exposed to different radiation dose rates while keeping the total dose constant. Irradiated samples, non-irradiated control samples, and reference standard solutions were analyzed using high performance liquid chromatography (HPLC) to determine the relative decomposition of irradiated nitrogen heterocycles, which can be used to extrapolate possible abundances during the time of the formation of the early Solar System.

CHAPTER TWO: HYDROTHERMAL CYANIDE REACTIONS

Introduction

The analyses of meteorites, daughter fragments of asteroid collisions, have revealed the presence of a variety of purine nitrogen heterocycles. These nitrogen heterocycles were determined to be extraterrestrial based on multiple lines of evidence as shown by Callahan *et al.*²⁴ For example, these same nitrogen heterocycles were also produced in laboratory ammonium cyanide reactions, which demonstrated a plausible abiotic synthetic pathway. However, these laboratory cyanide reactions were conducted at room temperature and do not necessarily reflect the conditions that all meteorite parent bodies may have experienced. Therefore, a study of ammonium cyanide reactions that have been heated to various temperatures was conducted in an effort to model the chemistry that occurred in meteorite parent bodies, particularly those that show some degree of hydrothermal alteration.

Experimental Methods

Materials

All glassware used in these experiments was wrapped in aluminum foil and baked out at 500 °C for 24 hours to remove any organic contamination. Some reagents were obtained from Sigma-Aldrich: adenine >99%, guanine >98%, uracil >99%, thymine >99%, cytosine >99%, xanthine, 5-aminouracil, 5-hydroxyuracil, orotic acid, and 5-aminoorotic acid. Potassium cyanide (KCN), purine, hypoxanthine, and 2,6-diaminopurine were obtained from Acros Organics. 8-aminoadenine (6,8-diaminopurine) was supplied by Tocris Bioscience. Ammonium chloride (NH₄Cl), glacial acetic acid, and HPLC grade

methanol was supplied by Fisher Chemical. All stock solutions were made using 18.2 M Ω -cm water (referred to as nanopure water) produced by a Barnstead Nanopure Diamond water purification system. All reagents used in these experiments were unmodified and used as received.

Sample Preparation

Aqueous solutions of 2 M ammonium chloride (NH₄Cl) and 2 M potassium cyanide (KCN) were made using nanopure water. 500 μ L of both NH₄Cl and KCN stock solutions were added to individual ampoules to give 1 mL of 1 M ammonium cyanide (NH₄CN) solution. The ampoules were then flame sealed with minimal air headspace and allowed to sit undisturbed in a fume hood for several months at room temperature. Ten identical room temperature reactions were produced for this study.

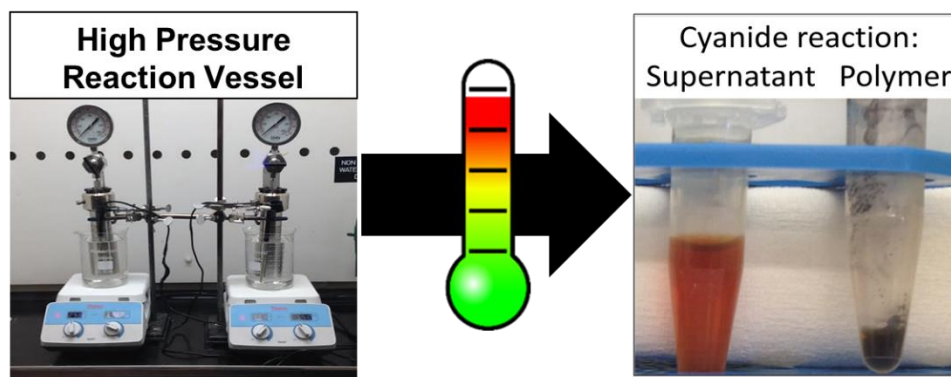
SAFETY WARNING: Cyanide reacts violently when heated releasing thermal energy and gas phase products. A high pressure reaction vessel was used to contain the reactions while behind a blast shield and inside of a fume hood.

For the *heated* reactions, stock solutions of 2 M ammonium chloride and 2 M potassium cyanide were added to an 8 mL glass vial producing 2 mL of 1 M ammonium cyanide solution. These glass vials were topped with an inverted 1 mL glass ampoule to help contain the cyanide polymerization reaction inside the vial. The vial-ampoule assembly was placed into a 200 mL Pyrex sleeve. Water was added to the Pyrex sleeve up to the same height as the NH₄CN solution inside the glass vial for better thermal contact. The Pyrex sleeve was then loaded into a high pressure reaction vessel (Parr Instrument Company general purpose pressure vessel Series 4750, rated to 350 °C and 3000 psi). Once sealed, the pressure vessel apparatus was degassed using a bath sonicator and vacuum

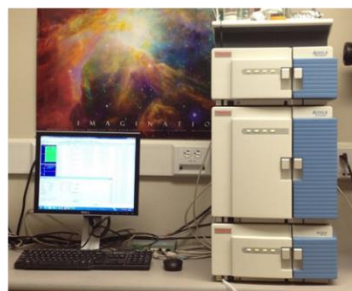
purge line for 5 minutes. After gas purging, the pressure vessel assembly was lowered into a temperature-conditioned silicone oil bath (50, 100, 150, or 200 °C) for times of 3, 24, and 72 hours. Each reaction was repeated 4 times. After heating, the cyanide reactions were cooled down and transferred to Eppendorf tubes. The cyanide reactions were centrifuged and the supernatant was decanted from the polymer. The polymer was washed with nanopure water, centrifuged, and then the nanopure water was removed; this step was performed a total of four separate times. The resulting black precipitate (referred to as cyanide polymer) was placed in a CentriVap micro IR vacuum concentrator at 40 °C until dry. The weight of the cyanide polymer was also recorded.

Instrumental Methods

The instrumentation used in this study include attenuated total reflectance Fourier transform infrared spectroscopy (ATR-FTIR) to determine differences in the bulk chemical properties of the supernatant and polymer. Qualitative analysis of the cyanide polymer was conducted by thermochemolysis gas chromatography-mass spectrometry (GC-MS). Tetramethylammonium hydroxide (TMAH, a quaternary ammonium salt) was used as a thermochemolysis and methylating agent. Qualitative analysis of the cyanide supernatant was conducted using high performance liquid chromatography (HPLC) with UV detection to identify and monitor nitrogen heterocycle production. The complete process for sample work-up and analysis is visualized in **Figure 2.1**.



Supernatant analysis



Polymer analysis

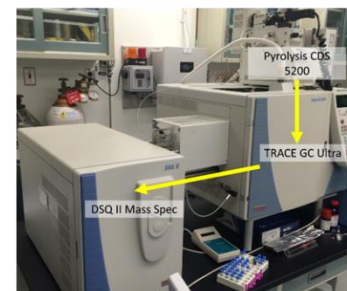


Figure 2.1. General scheme for reaction preparation, work-up and analysis. The supernatant was analyzed by ATR-FTIR and HPLC-UV and the polymer was analyzed by ATR-FTIR and TMAH-GC-MS.

Attenuated Total Reflectance Fourier Transform Infrared Spectroscopy

All IR spectra of the supernatant liquid and dried polymer were obtained on a Perkin Elmer Spectrum 100 FTIR Spectrometer with Universal ATR sampling accessory which is shown in **Figure 2.2**. U-ATR accessory was equipped with a zinc selenide/diamond crystal and set to triple bounce mode with a mean free path of 6 μm . The supernatant and polymer were separately placed on the universal sample accessory of an

ATR-FTIR instrument and IR spectra were acquired between 4000 and 650 cm^{-1} with 1 cm^{-1} resolution. IR spectra are an average of 50 scans. An air spectrum was recorded for background subtraction prior to sample analysis. IR spectra were plotted using Excel and Igor Pro plotting software.



Figure 2.2. Perkin Elmer spectrum 100 FTIR Spectrometer equipped with U-ATR accessory (with components labeled). This instrument was used for the analysis of the cyanide supernatant and polymer produced from several heated ammonium cyanide reactions.

Thermochemolysis Gas Chromatography-Mass Spectrometry

This technique utilizes a pyroprobe with product trap coupled to a gas chromatograph-mass spectrometer system. The system at NASA Johnson Space Center (Houston, Texas) consists of a CDS 5200 pyroprobe with a Tenax TA product trap and a Thermo Trace Ultra gas chromatograph (GC) coupled to a Thermo DSQ II single

quadrupole mass spectrometer (MS) shown in **Figure 2.3**. No additional preparation is required of the NH_4CN polymer samples prior to analysis. Silica glass capillaries and silica glass wool (used for sample containment in the pyroprobe) were baked at 500 °C for eight hours and subsequently stored at 200 °C until used. Approximately 1 - 3 mg of each NH_4CN polymer sample were loaded into glass capillaries and contained by glass wool inserted on both sides of the sample as shown in **Figure 2.4**; nearly equal amounts of polymer sample were loaded for semi-quantitative analysis. Each sample capillary is injected with 5 μL of 25 wt% TMAH in methanol. The sample capillary is then inserted into a platinum resistance heating coil in the pyroprobe system. The sample is then heated to 250 °C (or 500 °C) for 10 minutes while helium is flowed through the system at 20 mL/min and the products are removed to the Tenax trap held at 40 °C. Products from the polymer collect at the trap for the entire duration of the procedure, leaving no products in the heated zone. After 10 minutes the contents of the trap are thermally desorbed at 350 °C and released to the GC inlet. All heated zones in the GC and MS are maintained at 250 °C (including the GC inlet, GC to MS transfer line, and MS ion source). The GC oven was ramped between 60 and 300 °C at a rate of 4 °C/min then held at 300 °C for five minutes (65 minute total duration). Mass scans were collected between 10 to 600 amu at a rate of one scan per second. Electron ionization (EI) at 70 eV was used with a single quadrupole mass analyzer working in positive (+) ion mode. Typically, multiple scans were averaged to produce a mass spectrum, which also included a background subtraction (using data near the peak of interest).

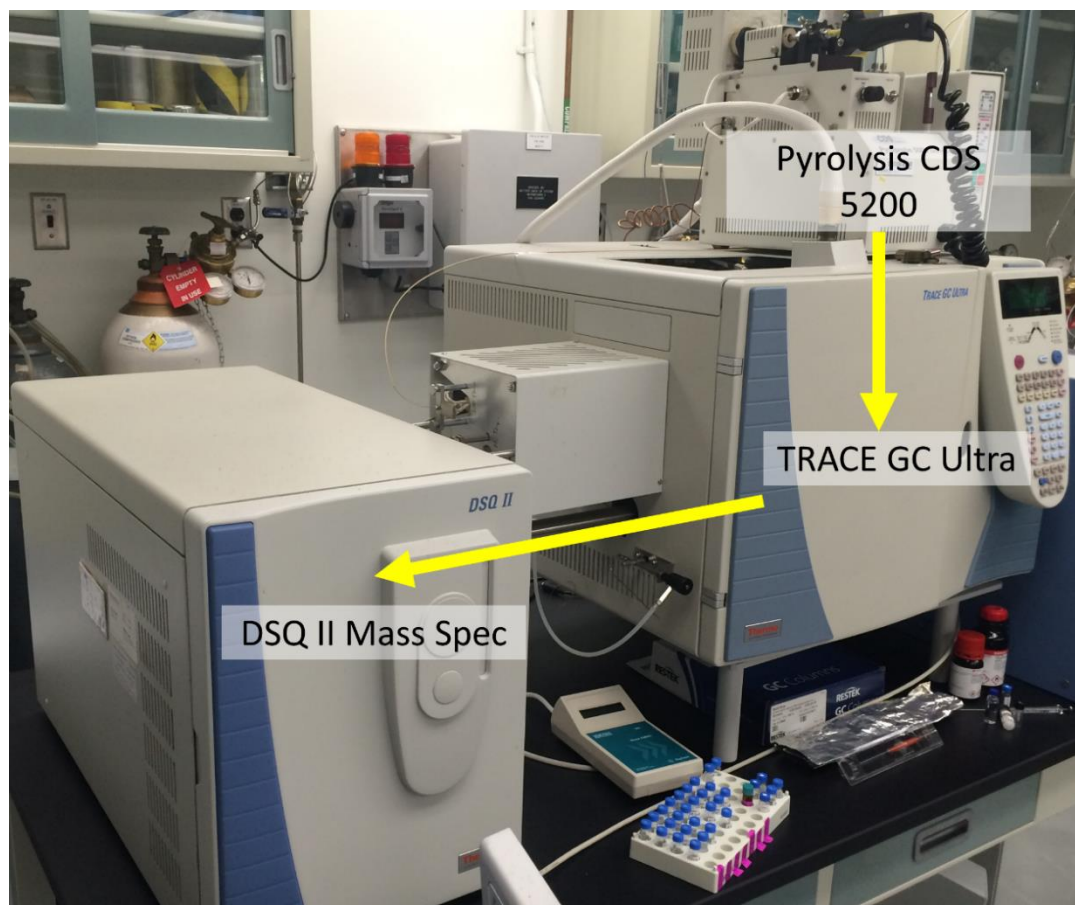


Figure 2.3. Thermochemolysis GC-MS (with components labeled) used for the analysis of cyanide polymer. The system includes a pyroprobe with a Tenax TA product trap and a gas chromatograph coupled to an electron ionization source (EI) held at 70 eV and a single quadrupole mass spectrometer. Photo courtesy of Dr. Darren Locke and Dr. Aaron Burton of the NASA Johnson Space Center.

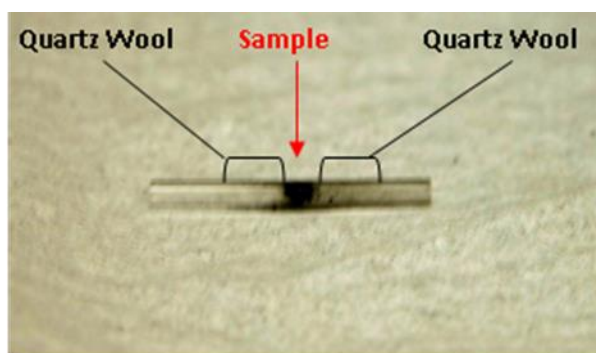


Figure 2.4. Thermochemolysis sample unit. Polymer samples are placed inside of a glass capillary tube with 5 μL of TMAH solution. The capillary tube is then heated to 250 $^{\circ}\text{C}$ inducing a chemical reaction between TMAH and the cyanide polymer. This causes the polymer to decompose into smaller molecular fragments which become methylated and thus are more amenable to GC-MS analysis.

Thermochemolysis with TMAH results in bond cleavage of the polymer along with *in situ* methylation of products, which can be used to better understand the complex nature of the ammonium cyanide polymer (and how increasing reaction temperature changes this structure). As a result, all of the nitrogen heterocycles searched for in this study have (potentially) several derivatized masses to search for in the total ion chromatograms obtained from the GC-MS. These masses along with the parent mass and empirical formula for the compounds are listed in **Table 2.1**. All masses shown are nominal mass of the compound and increase by 14 amu with each methyl derivative. Final identification of compounds was made using the NIST/EPA/NIH Mass Spectral Library (NIST 2014) where the main library contains EI mass spectra for 242,466 chemical compounds. Best compound matches were evaluated using two factors: SI (“a direct matching factor for the unknown and the library spectrum”) and RSI (“a reverse search matching factor ignoring any peaks in the unknown that are not in the library spectrum”). With these matching factors, an SI-RSI score of 900 or greater is an excellent match, 800-900 is considered a good match, 700-800 is considered a fair match, 600-700 is considered a fair/poor match, and <600 is considered a poor match. In the discussion, we focus mainly on compounds with SI and RSI scores of >700, which would be considered more reliable identifications.

Previously, TMAH-based thermochemolysis GC-MS was used to analyze cyanide polymer synthesized under ambient (room temperature) conditions and revealed a complex suite of organics as demonstrated by Matthews and Minard.⁷ Here, TMAH-based thermochemolysis GC-MS was used to analyze the cyanide polymer that was synthesized in aqueous NH₄CN heated at different temperatures for 72 hours.

Table 2.1. Nominal mass data and empirical formulas for nitrogen heterocycle thermochemolysis products. Derivatization of thermochemolysis products using TMAH provides several methylated, dimethylated, trimethylated, and tetramethylated polymer fragments. All of these masses were searched for within several total ion chromatograms.

Nitrogen heterocycle Nominal Derivative Mass Data					
N-Heterocycle	Formula	Parent Mass	1st Derivative	2nd Derivative	3rd Derivative
Adenine	C ₅ H ₅ N ₅	135	149	163	177
Cytosine	C ₄ H ₅ N ₃ O	111	125	139	153
Guanine	C ₅ H ₅ N ₅ O	151	165	179	193
Thymine	C ₅ H ₆ N ₂ O ₂	126	140	154	168
Uracil	C ₄ H ₄ N ₂ O ₂	112	126	140	154
Purine	C ₅ H ₄ N ₄	120	134	148	162
2,6-diaminopurine	C ₅ H ₆ N ₆	150	164	178	192
6,8-diaminopurine	C ₅ H ₆ N ₆	150	164	178	192
Hypoxanthine	C ₅ H ₄ N ₄ O	136	150	164	178
Xanthine	C ₅ H ₄ N ₄ O ₂	152	166	180	194
5-aminouracil	C ₄ H ₅ N ₃ O ₂	127	141	155	169
5-hydroxyuracil	C ₄ H ₄ N ₂ O ₃	128	142	156	170
Orotic acid	C ₅ H ₄ N ₂ O ₄	156	170	184	198
5-aminoorotic acid	C ₅ H ₅ N ₃ O ₄	171	185	199	213
4,5-dihydroxypyrimidine	C ₄ H ₃ N ₂ O ₂	111	125	139	153
s-Triazine	C ₃ H ₃ N ₃	81	95	109	123
Cyanuric acid	C ₃ H ₃ N ₃ O ₃	129	143	157	171
Ammeline	C ₃ H ₅ N ₅ O	127	141	155	169
Ammelide	C ₃ H ₄ N ₄ O ₂	128	142	156	170
Melamine	C ₃ H ₆ N ₆	126	140	154	168

High Performance Liquid Chromatography

The supernatant liquid was loaded into a 1 mL syringe (Covidien Monoinject) and filtered into an HPLC vial using a syringe filter (Whatman PURADISC 25 AS with 0.45 μm polyethersulfone membrane in a polypropylene housing). All supernatants of the cyanide reactions produced in this study were analyzed using a Thermo Scientific high performance liquid chromatograph equipped with an ACCELA 600 pump, ACCELA autosampler, and ACCELA photodiode array UV-Vis (PDA) 80 Hz detector as shown in **Figure 2.5**. N-heterocycle reference standards were dissolved in 0.1 M HPLC grade ammonium hydroxide to produce ~3 mM nitrogen heterocycle stock solutions. These stock

solutions were then successively diluted to obtain 1, 10, 50, and 100 μM solutions for determination of the linear range of instrument response to analyte concentration as well as the limit of detection (LOD), which was found to be ~ 10 picomoles on the column. Reference standard solutions were also used to determine retention times of nitrogen heterocycles and their UV spectra.

Nitrogen heterocycle separation was achieved with two (sequential) Phenomenex Luna 5 μm phenyl-hexyl reverse phase columns (4.6 mm \times 250 mm; 100 angstrom pore size). The column oven was maintained at 40 $^{\circ}\text{C}$. Mobile phase A was composed of 10 mM ammonium formate buffer at a pH of 3.85. Mobile phase B was 100% LC/MS grade methanol (less than 2 mAU between 200-400 nm). Ammonium formate buffer was prepared via NH_4OH titration of the 10 mM formic acid solution to pH 3.85. All reagents used for making the buffer solutions were HPLC grade and not filtered.

Initial conditions were 0% B at 0 minutes and followed by a linear gradient to 50% B in 50 minutes. From 50 to 52 minutes, the solvent was adjusted to 100% B and held at 100% B until 82 minutes (30 minutes) to flush away any remaining organics. From 82 to 84 minutes the solvent was adjusted to 100% A and held at 100% A until 104 minutes (20 minutes) to establish initial column conditions. The flow rate was kept at 300 $\mu\text{L}/\text{min}$ during the entire HPLC run. An injection volume of 10 μL was used for each sample and standard. Each sample and standard was injected three times for triplicate analyzes. The PDA detector recorded the UV spectrum from 200-400 nm; for nitrogen heterocycle analysis, the wavelength of 260 nm was typically monitored.

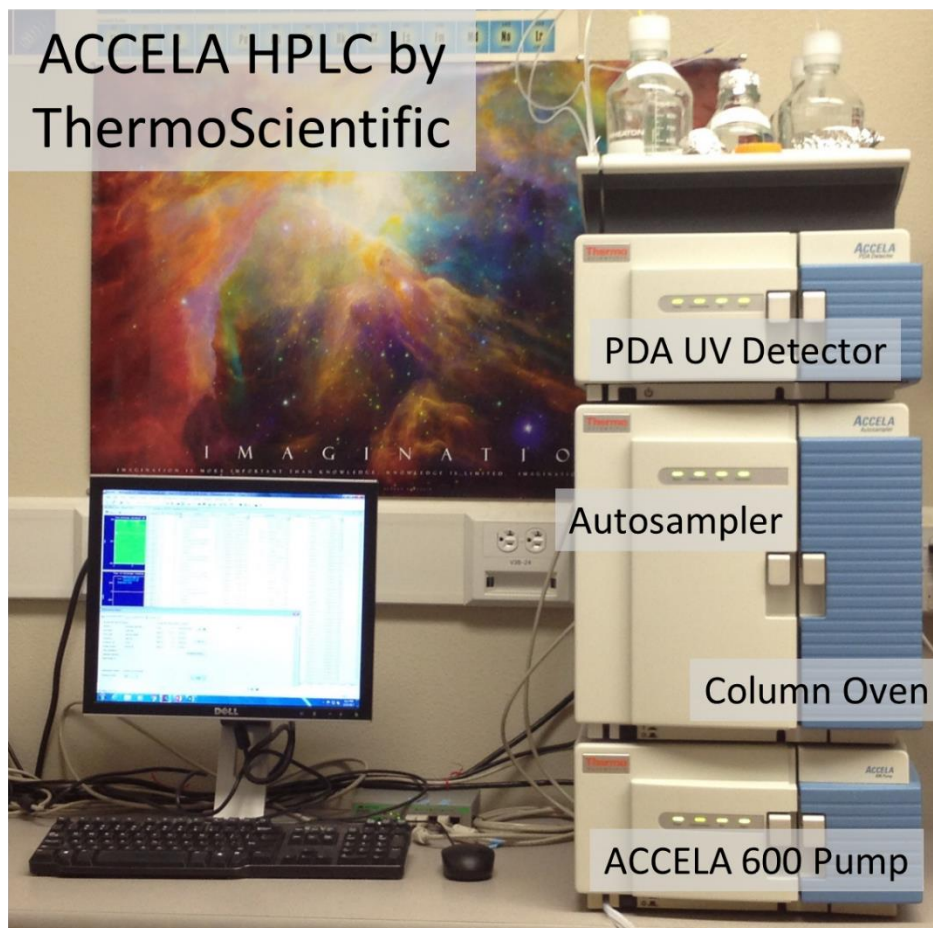


Figure 2.5. HPLC-UV instrument (with components labeled) used for the analysis of supernatant portions of heated ammonium cyanide reactions. Nitrogen heterocycles were typically monitored at 260 nm, although the full spectrum from 200-400 nm was acquired by the PDA detector.

Results and Discussion

Initial Observations of Cyanide Reactions

A large set of 1 M NH_4CN reactions was prepared at different temperatures (50, 100, 150, and 200 °C) and times (3, 24, and 72 hours). The entire sample set consisted of 13 NH_4CN reactions, which also included a 6-month room temperature reaction. The initial clear/colorless solution had a pH of ~9.5 as determined by pH paper. After reaction, the color of the supernatant ranged from dark red at room temperature to bright yellow at 200 °C. Additionally, there was a general trend in the heated reactions that polymer mass

increased as reaction temperature increased, which is listed in **Table 2.2**. Percent polymer in terms of % wt/wt, determined based on the initial mass of cyanide in the reaction vial, is also listed in **Table 2.2**. Ultimately, the 6-month room temperature reaction yielded the highest mass of polymer, which suggests that this reaction may have progressed further, compared to the short-term heated reactions.

Table 2.2. Polymer mass in mg (and % wt/wt) of each cyanide reaction. The six month old room temperature reaction yielded a cyanide polymer mass of 15.2 mg and 29.5% wt/wt.

Mass, mg (% wt/wt)			
Temperature	3 Hours	24 Hours	72 Hours
50 °C	0.4 (0.8)	0.5 (1)	0.5 (1)
100 °C	1 (1.9)	0.4 (0.8)	0.4 (0.8)
150 °C	1 (1.9)	1 (1.9)	3.8 (7.2)
200 °C	1.8 (3.4)	3.2 (6.1)	3.4 (6.5)

Infrared Spectroscopy of the Cyanide Supernatant and Polymer

Figure 2.6 shows IR spectra representative of the cyanide polymer (black trace) and supernatant (orange trace) obtained from a six-month room temperature reaction produced during this study. Infrared spectra of the cyanide polymer gathered in this study correspond well to reported literature.⁴³⁻⁴⁶

Within these spectra are three distinct regions of IR absorbance bands, which are common to the liquid and solid. In the higher energy portion of the IR spectrum, there appear two strong and broad absorbance peaks attributed as primary (and possibly secondary) nitrogen-hydrogen bond stretching. These absorbance bands are associated with the amine functional group contained within the supernatant and polymer. The nitrile functional moiety (carbon-nitrogen triple bond absorbance) in the supernatant and polymer can be located in the middle of the two spectra at roughly 2150 cm^{-1} . The last discernable

pair of peaks represented in both fractions is located near 1640 cm^{-1} and is attributed to carbon-nitrogen double bond absorbances associated with imine functional groups of the cyanide organic products contained in the supernatant and composing the backbone structure of the cyanide polymer. The remaining absorbances lie within the fingerprint regions of the spectra. For the polymer, there is a complex hodgepodge of absorbance bands likely associated with variations in substitution of carbon-nitrogen single and double bonds. This region has been reported in the literature as being attributed to polypeptides or polyamidines.¹⁰ Further analysis of this region may be possible with chemometrics software to assist in identifying additional structural elements of the cyanide polymer; however, the intention of IR analyses of these reactions is qualitative in nature and intended to reveal changes in the bulk properties of the cyanide products as the reactions are exposed to increasing temperatures. Therefore, more involved software analysis of the IR spectra was not considered necessary.

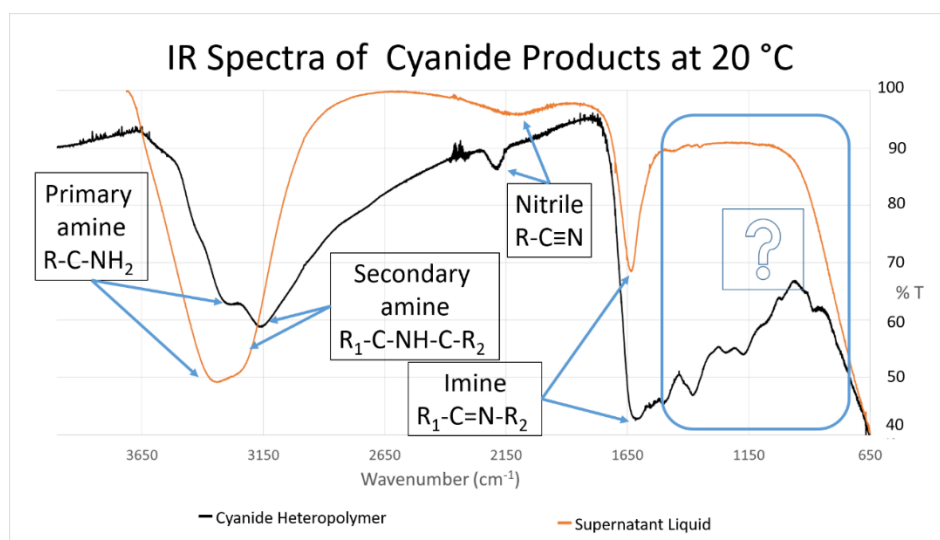


Figure 2.6. IR spectra of supernatant (orange) and polymer (black) obtained from a 6-month, room temperature NH_4CN reaction. Both supernatant and polymer contain primary and secondary amines, nitriles, and imines. The blue boxed region contains a series of complex absorbances typically associated with C-C and C-N single and double bond stretching and bending vibrational modes.

Figure 2.7 is a series of overlaid supernatant spectra that have reacted for 72 hours. Each spectrum represents a separate reaction heated incrementally by 50 °C to 200 °C. Peak (A) at 1631 cm^{-1} is the imine peak and is the same in all the spectra regardless of temperature. As the temperature is increased, four additional peaks develop within the spectra. The second peak (B) at 1585 cm^{-1} is attributed a splitting in the imine peak (A) associated with a change in the structure of the supernatant. With an increasing prominence of a new structural motif in the supernatant, some of the imine functional groups are bound to this new structure and as a result their absorbance is shifted to slightly lower energy. This results in a splitting in the imine peak (A) to produce imine peak (B) at higher temperatures. The remaining peaks (C, D, and E) are attributed to these changes in the structure of the supernatant as variations in the substitution patterns as well as single and double bond character in the supernatant.

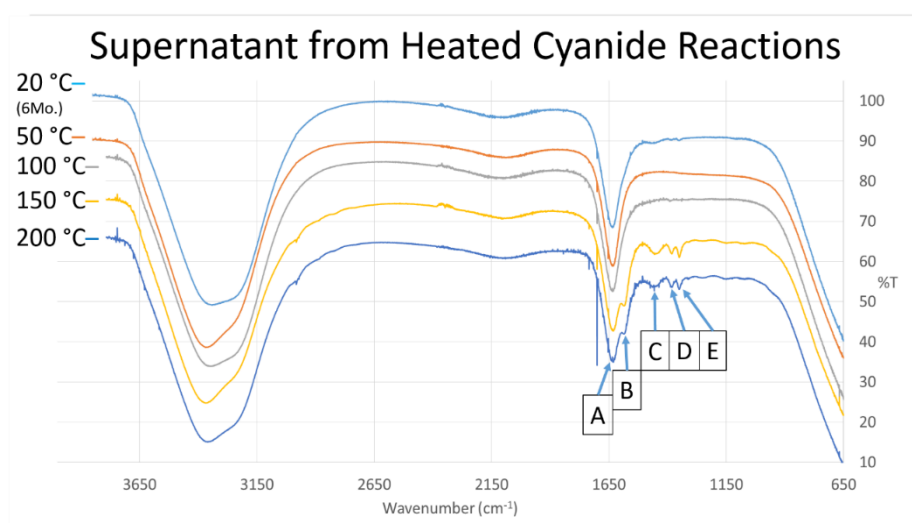


Figure 2.7. IR spectra of supernatant from NH_4CN reaction heated at different temperatures for 72 hours. Peaks (A) 1631 cm^{-1} , (B) 1585 cm^{-1} , (C) 1454 cm^{-1} , (D) 1382 cm^{-1} and (E) 1350 cm^{-1} are labeled.

Figure 2.8 represents overlaid polymer spectra with increasing ammonium cyanide reaction temperatures. As the temperature is increased, the amine absorbance bands show

no significant changes. The most significant differences in the spectra occur in the fingerprint region at less than 1640 cm^{-1} . Here, the prominent peak in the room temperature spectrum at 1640 cm^{-1} corresponds to imine groups and remains present throughout the temperature series. At higher temperatures, the imine peak becomes a shoulder to absorbance bands at lower wavenumbers that develop with increasing reaction temperature.

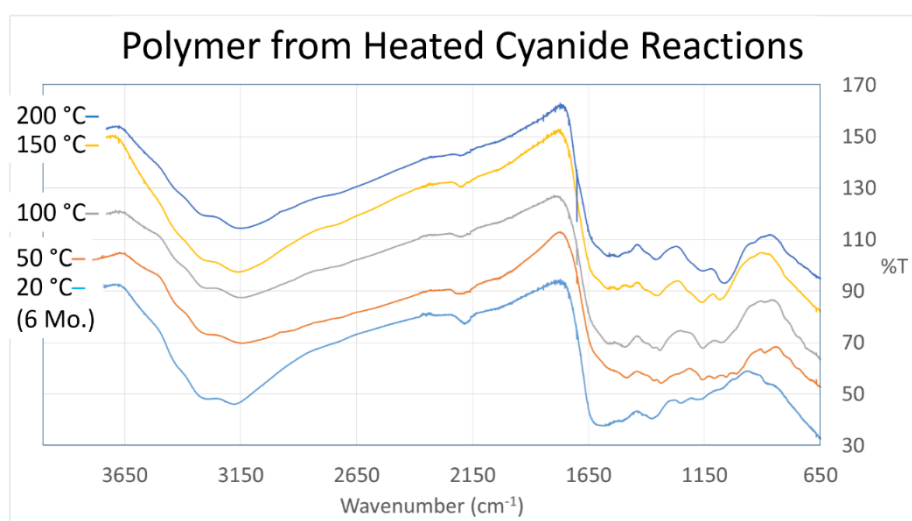


Figure 2.8. IR spectra of polymer obtained from NH_4CN reactions heated at different temperatures for 72 hours. The imine peak at 1631 cm^{-1} is present in all of the spectra. However, at increased reaction temperatures, there is a shift in the intensity of the absorbance bands between $1600\text{--}1000\text{ cm}^{-1}$ as the reaction temperature is increased.

Additionally, there is a noticeable increase in absorbance bands between $1500\text{--}1000\text{ cm}^{-1}$ attributed to substitution and single/double bond variations in the C-C and C-N network composing the polymer structure. This region of IR spectra is also associated with vibrational stretching and bending modes for several different functional groups. This includes amines, amides, alkenes, aromatics, and imines. Similar to the peak development observed in the supernatant, the development of a new structural motif in the polymer may explain these increases in absorbances in the fingerprint region of the polymer spectra.

The last significant variation of the cyanide polymer due to increasing temperature is identified in a close-up of the cyanide peak around 2200 cm^{-1} . Shown in **Figure 2.9** is an enlarged view of the cyanide polymer nitrile peak obtained from heated reactions for 72 hours at different temperatures. Peak shifting is observed within the nitrile peak, absorbing at 2180 cm^{-1} in the room temperature spectrum to a higher absorbance frequency of 2200 cm^{-1} in the $200\text{ }^{\circ}\text{C}$ spectrum. With this shifting a peak develops at 2170 cm^{-1} , which is assigned as an isonitrile peak based on the literature where ammonium cyanide polymer was produced under similar conditions. However, this study by Mutsukura and Akita. was not analyzing polymers produced at different temperatures.⁴⁵ An alternative explanation of this peak splitting of the nitrile functional group could be changes in bonding characteristics of the cyanide polymer as the temperature of reaction increases (e.g., a shift from one type or mixture of structures dominated by polyamidines, polypeptides, or polynucleobases to another structure). Likewise, this structural change is thought to have an effect on the nitrile peak. As the reaction with cyanide continues, free cyanide reacts with different motifs in the polymer to produce a nitrile functional group and the associated absorbance peaks having similar but slightly different absorbance energies. As the new structure forms, cyanide may react with and bind to new motifs. This is thought to result in splitting of the nitrile peak.

All of the observations shown are representative of changes in the *bulk* properties of the cyanide products with increasing temperature (for the NH_4CN reaction); however, there are questions that still remain. What is happening on a molecular level in both supernatant and polymer? How do these changes affect nitrogen heterocycle production?

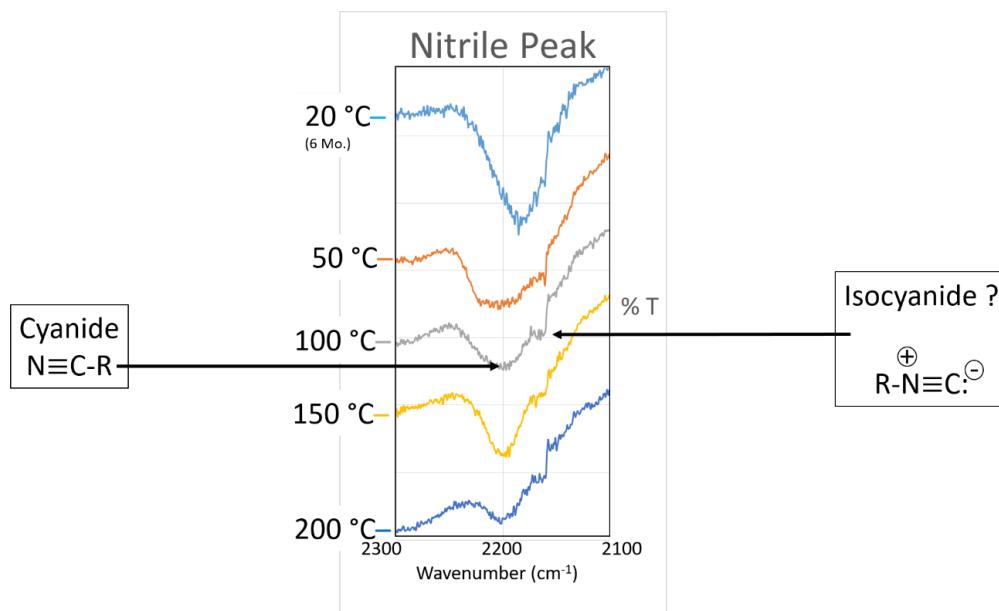


Figure 2.9. Close-up of IR spectra of polymer obtained from NH_4CN reactions heated at different temperatures for 72 hours. A shift in absorbance from 2180 to 2200 cm^{-1} reveals the development of an additional peak at 2170 cm^{-1} at higher temperature.

Thermochemolysis of Cyanide Polymer Using TMAH GC-MS

Polymer samples (>5 mg each) of the 72-hour temperature series were shipped to NASA Johnson Space Center (Houston, Texas) for thermochemolysis gas chromatography mass spectrometric analysis (TMAH-GC-MS). TMAH cleaves labile functional groups (e.g., amidine, amide, and imine) and methylates the resulting products *in situ*.⁷ As a result, methylated compounds are likely to be the result of derivatization; however, cleavage of naturally methylated compounds from the polymer cannot be completely ruled out. Shown in **Appendix A** is a complete tabulation of all the compounds detected in the mass spectral data of the polymer samples with fits >700 along with methylated and non-methylated structures of these compounds.

The total ion chromatogram obtained from the room temperature polymer sample is shown in **Figure 2.10** and was analyzed peak by peak using the NIST 2014 MS database. Additionally, masses corresponding to methyl-derivatized nitrogen heterocycles were

searched for by plotting extracted ion chromatograms, which can result in better examination of the data.

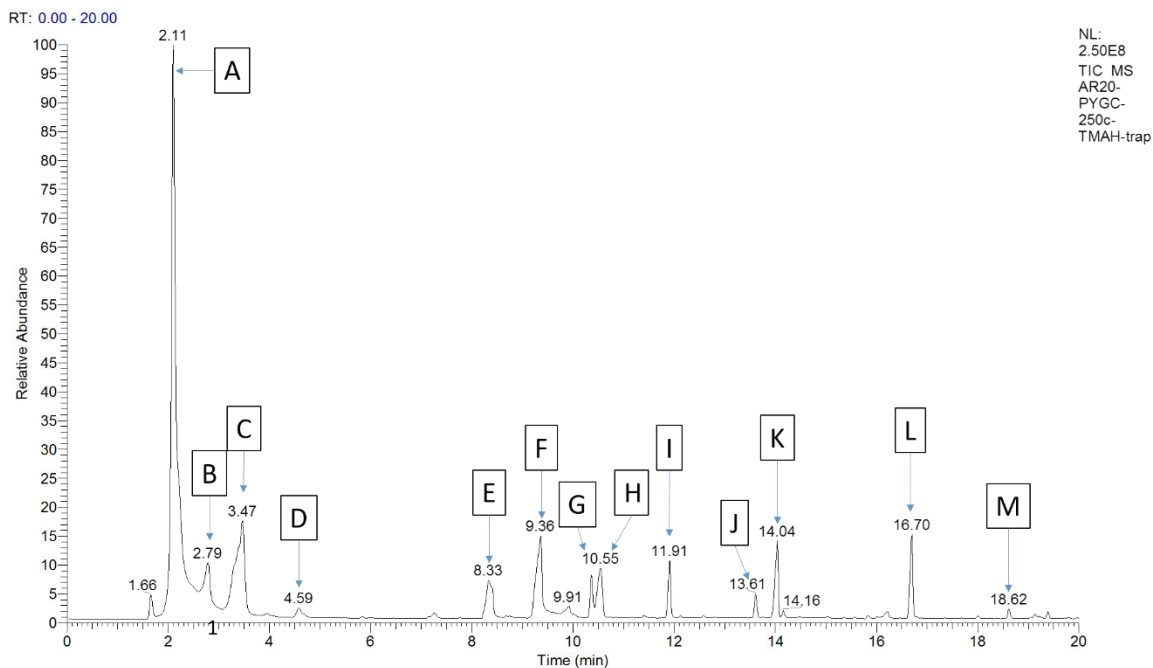


Figure 2.10. GC-MS total ion chromatogram with thermochemolysis products of room temperature cyanide polymer labeled: (A) trimethylamine, (B) formamide, (C) N,N'-dimethylformamide, (D) aminoacetonitrile, (E) N,N'-dimethylurea, (F) trimethylurea, (G) diamide, (H) N,N'-dimethyloxamide, (I) formyltrimethylurea, (J) 1-methyl-dihydrouracil, (K) 1,3-dimethyl-2,4,5-trioxoimidazolidine, (L) tetramethylurea, and (M) 4-dimethylaminopyridin-2-amine.

Within this chromatogram, several compounds were identified with good matches to NIST library spectra including some previously reported in HCN polymers by Matthews and Minard such as aminoacetonitrile, cyanamide (as the dimethyl derivative), formamide (as the methyl and dimethyl derivatives), urea (as the dimethyl, trimethyl, and tetramethyl derivatives), adenine (as the methyl, dimethyl, and trimethyl derivatives), xanthine (as the trimethyl derivative, caffeine) and cyanuric acid (as the trimethyl derivative).⁷ Additional compounds were also identified in this study including (1) oxamide (as the dimethyl derivative), (2) dihydrouracil (as the methyl derivative) and hypoxanthine (as the dimethyl

derivative), which are in the class of pyrimidines and purines, (3) 2,4-diaminopyridine (as the dimethyl derivative), which is a 6-membered nitrogen heterocycle, and (4) 2,4,5-trioxoimidazolidine (as the dimethyl derivative) and 2,4-imidazolidinedione (as the trimethyl derivative), which are both 5-membered nitrogen heterocycles. The complex suite of TMAH thermochemolysis-derived compounds reinforces the concept that the cyanide polymer is complex and heterogeneous in nature. **Table 2.3** lists the compounds identified in the room temperature polymer sample.

Shown in **Figure 2.11** are overlaid total ion chromatograms of the four cyanide polymer samples reacted at increasing temperatures. In this figure, one can easily visualize the changes in compound production with increases in the reaction temperature. After establishing the identity of these compounds, thermochemolysis-derived compounds of the polymer can be tracked with respect to reaction temperature.

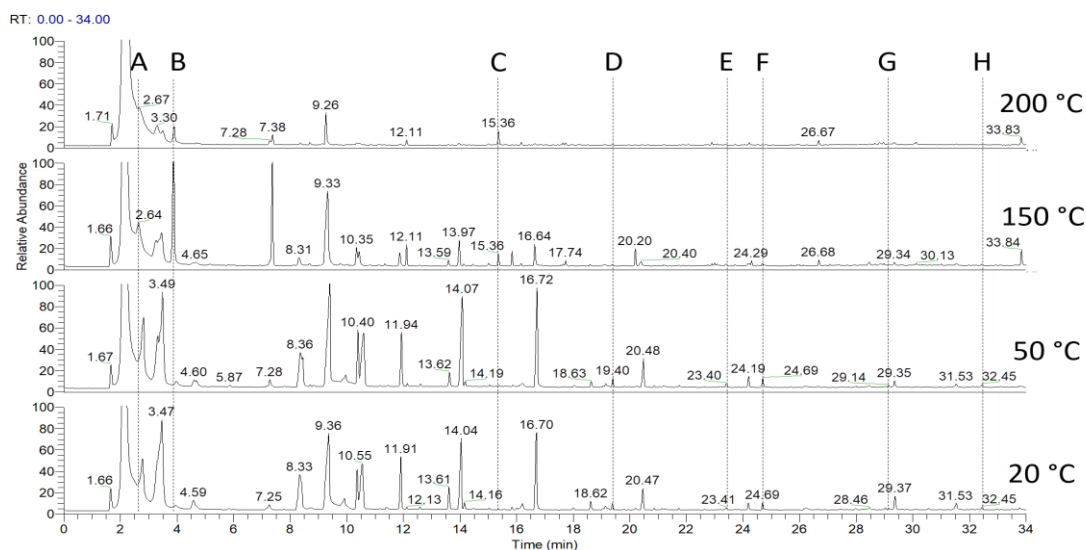


Figure 2.11. Total ion chromatograms of polymer samples synthesized at different reaction temperatures for 72 h that have been measured by thermochemolysis GC-MS. Aromatic and heterocyclic compounds are tracked throughout the entire temperature series: (A) benzene, (B) anthracene/phenanthrene, (C) m-di-t-butyl-benzene, (D) trimethyl-cyanuric acid, (E) 1,3-dimethyl-5,6-diamino-uracil, (F) 1,7-dimethyl-hypoxanthine, (G) N6,N6',N9-trimethyl-adenine, and (H) 1,3,7-trimethyl-xanthine.

Table 2.3. Compounds identified in room temperature polymer samples as determined by TMAH-GC-MS and comparison to NIST/EPA/NIH Mass Spectral Library.

Compounds Identified in the Room Temperature Cyanide Polymer by TMAH-GC-MS				
Retention Time (min)	Compound Name	SI	RSI	FIT
2.11	N,N-dimethylmethylamine (by-product of TMAH)	908	911	Excellent
2.66	benzene	816	882	Good
2.79	Formamide	706	848	Fair
3.47	N,N-dimethylformamide	867	917	Good
3.9	anthracene	882	919	Excellent
4.59	aminoacetonitrile	808	816	Good
5.83	1H-pyrazole, 3-ethyl-4,5-dihydro-	610	723	Fair/Poor
8.33	N,N-dimethylurea	736	750	Fair
9.36	trimethylurea	758	768	Fair
9.91	N,N'-dimethylurea	731	780	Fair
10.36	diamide	698	823	Fair
10.55	N,N'-dimethyloxamide	881	934	Good
11.16	1-methyl-1H-imidazole-2-carbonitrile	702	796	Fair
11.41	1,3-cyclopentanedione, 2-methyl (native methyl?)	630	654	Fair/Poor
11.91	urea, formyltrimethyl-	688	690	Fair/Poor
12.59	4,6-dimethyl-3,5-dioxo-2,3,4,5-tetrahydro-1,2,4-triazine	737	834	Fair
13.61	1-methyl-dihydrouracil	783	791	Fair/Good
14.04	1,3-dimethyl-2,4,5-trioxoimidazolidine	857	905	Good
14.16	2,4-imidazolidinedione, 3,5,5-trimethyl	784	847	Fair
14.47	N-ethyl-hexahydro-1H-azepine	721	808	Fair
15.02	6-azathymine, bis(methyl) ether	728	789	Fair
15.37	m-di-tert-butylbenzene	821	876	Good
15.57	3-methyl-dihydrouracil or 1-	649	705	Fair/Poor
15.82	4-piperidinone, 1,3-dimethyl-	694	736	Fair/Poor

Table 2.3 Continued. Compounds identified in room temperature polymer samples as determined by TMAH-GC-MS and comparison to NIST/EPA/NIH Mass Spectral Library.

Compounds Identified in the Room Temperature Cyanide Polymer by TMAH-GC-MS				
Retention Time (min)	Compound Name	SI	RSI	FIT
16.22	2-methyliminoperhydro-1,3-oxazine	700	807	Fair
16.7	urea, tetramethyl-	782	864	Fair
16.7	ethylenediamine, N,N'-diethyl-N,N'-dimethyl-	728	789	Fair
18.62	4-dimethylaminopyridin-2-amine	729	751	Fair
19.13	1-methyl-1H-imidazole-2-carbonitrile	693	813	Fair/Poor
19.13	7H-pyrrolo[2,3-d]pyrimidin-4-amine	654	698	Fair/Poor
19.23	2-amino-4,6-dimethylpyridine	690	751	Fair/Poor
19.38	cyanuric acid, trimethyl-	890	912	Good
20.47	2,5,5-trimethyl-3-oxo-pyrroline, 1-oxide	641	685	Fair/Poor
20.85	5,6-dimethyl-2-benzimidazolinone	680	703	Fair/Poor
23.41	1,3-dimethyl-5,6-diaminouracil	609	662	Fair/Poor
24.19	6-azathymine, bis(methyl) ether	702	716	Fair
24.69	1,7-dimethyl-hypoxanthine	719	758	Fair
26.24	N1-methyladenine	640	756	Fair/Poor
27.99	N6,N9-dimethyladenine	746	888	Fair
29.04	N6,N6',N9-trimethyladenine	802	841	Good
29.37	1,3,7-trimethylxanthine	595	641	Poor
31.53	1-iso-propyl-3,6-diazahomoadamantan-9-one	579	658	Poor
32.45	1,3,7-trimethylxanthine (caffeine)	792	838	Fair/Good
34.48	hexadecanoic acid, methyl ester (C16:0)	888	900	Good
35.36	hexadecanoic acid (C16:0)	689	751	Fair/Poor
39.17	octadecanoic acid, methyl ester (C18:0)	920	929	Excellent
35.36	octadecanoic acid (C18:0)	837	854	Good

Figures 2.12-2.15 provide an analysis of extracted ion chromatograms; there appears to be a general decrease in abundances (peak areas) of nitrogen heterocycles as the temperature of the NH_4CN reaction increased. **Figure 2.12** shows the reduction in purine nitrogen heterocycles that corresponds to increasing reaction temperatures. This trend extended to many other non-N-heterocyclic compounds as well (**Figure 2.13**). Displaying the reverse trend observed in **Figure 2.14**, there is an increase in abundance of aromatic products such as benzene and anthracene/phenanthrene as the temperature of the NH_4CN reaction increased. Benzene has the most pronounced increase in abundance at 150 °C which then decreases at 200 °C. This production is still higher than that produced in the room temperature reactions. However, the sharp increase followed by a pronounced decrease in benzene production cannot be ignored. Reasons for this potential discrepancy could result from variation in sample size (1 – 3 mg) and/or to benzene product fragments from other compounds at the associated retention time (EI source may fragment compounds like m-di-t-butyl-benzene).

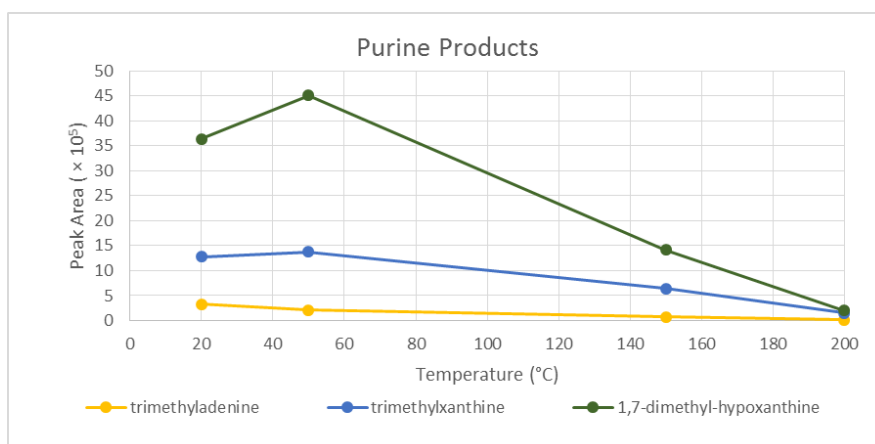


Figure 2.12. Relative peak area versus temperature plots of thermochemolysis products of cyanide polymer produced from heated ammonium cyanide reactions. Peak area was determined from the GC-MS extracted ion chromatogram at the appropriate m/z. Purine heterocycles decrease in abundance as reaction temperature is increased.

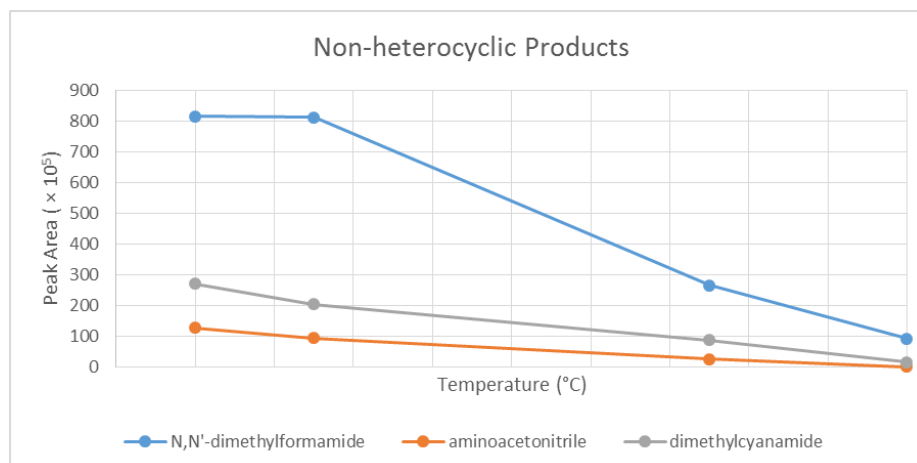


Figure 2.13. Relative peak area versus temperature plots of thermochemolysis products of cyanide polymer produced from heated ammonium cyanide reactions. Peak area was determined from the GC-MS extracted ion chromatogram at the appropriate m/z. Non-heterocyclic products decrease in abundance with increased reaction temperature.

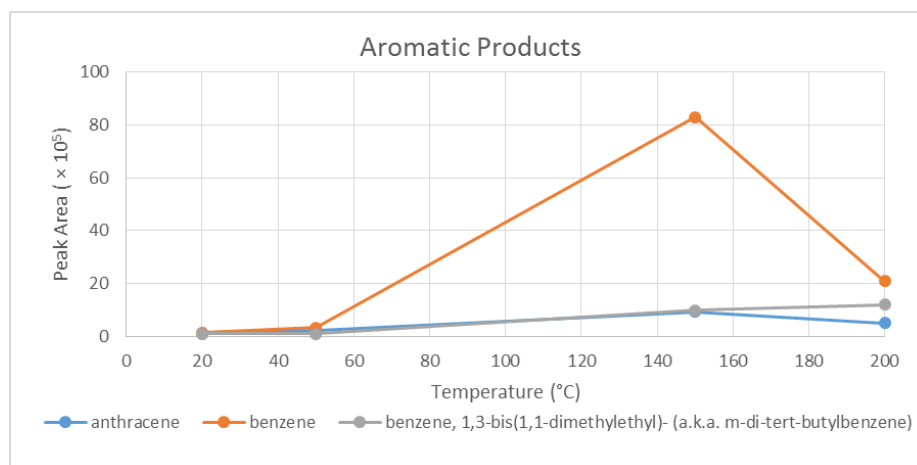


Figure 2.14. Relative peak area versus temperature plots of thermochemolysis products of cyanide polymer produced from heated ammonium cyanide reactions. Peak area was determined from the GC-MS extracted ion chromatogram at the appropriate m/z. Aromatic compounds increase in abundance as the reaction temperature is increased.

To highlight these trends, a comparison of adenine (nucleobase) and benzene (aromatic) is shown in **Figure 2.15**. The extracted ion chromatograms of adenine are shown on the left and are all scaled to the room temperature extracted ion chromatogram. The extracted ion chromatograms of benzene are shown on the right and are all scaled to the

150 °C extracted ion chromatogram. It is possible that higher reaction temperatures (for NH_4CN) have produced char, highly aromatic coal-like structure, from the cyanide polymer because multiple aromatic species were observed to increase with increasing reaction temperature.

The products that can be released from cyanide polymer are thought to play an important role in prebiotic chemistry on early Earth. *One important observation from this study is that many of these products (e.g., Nitrogen heterocycles) are not “better preserved” in cyanide polymer form compared to the supernatant form (the latter will be discussed in the next section) and products that can be released from cyanide polymer will strongly depend on initial reaction conditions.*

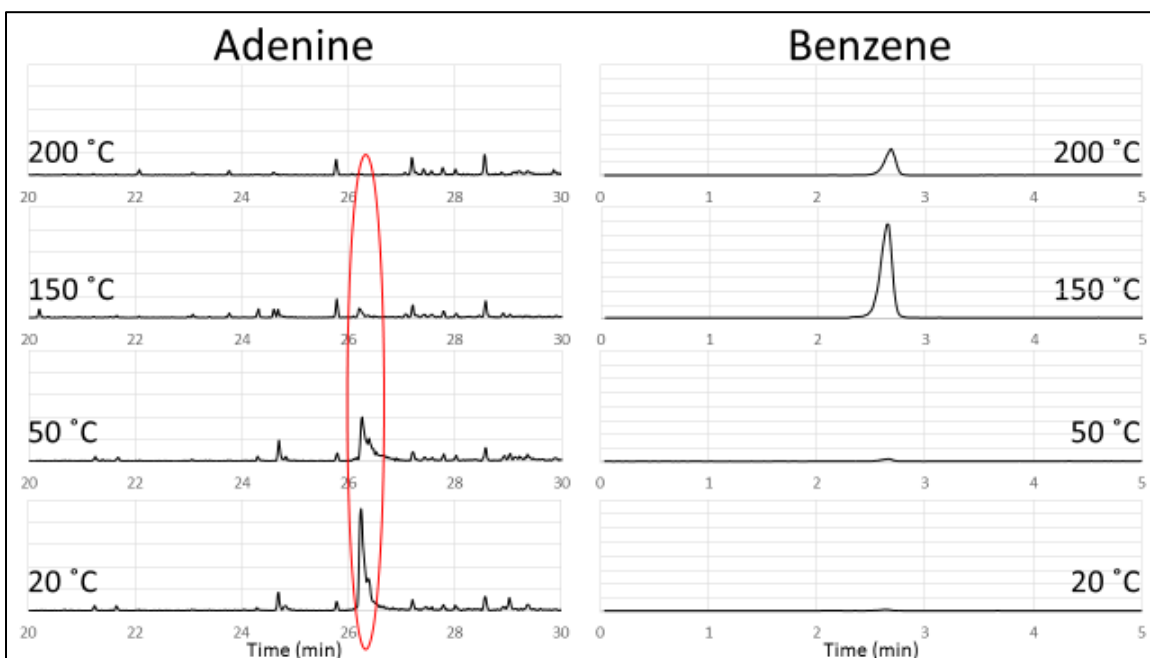


Figure 2.15. Comparison of extracted ion chromatograms of adenine (nucleobase) and benzene (aromatic) production in thermochemolysis products of NH_4CN polymers. Relative peak area for adenine decreases while the relative peak area for benzene increases, both with respect to increasing NH_4CN reaction temperature that produced the cyanide polymer.

Qualitative Identification of Nitrogen heterocycles Using HPLC

In this study, HPLC with UV detection was used for qualitative identification of nitrogen heterocycles. Initially, 15 nitrogen heterocycles were chosen for analysis as they are either known to be produced in room temperature cyanide reactions or are found in formic acid extracts of meteorites. Many nitrogen heterocycles, including nucleobases, have a significant UV absorbance at 260 nm or nearby. The exception to this was *s*-triazine whose lambda max is near 200 nm and has virtually no detectable absorbance at the monitoring wavelength of 260 nm. Therefore, triazines were not searched for in the supernatant samples due to current instrumental limitations. Triazines have been previously shown to be produced in cyanide reactions and have been identified in meteorite extracts.⁴⁷

As most of the products of cyanide chemistry are produced in relatively low abundance, have similar chemical properties, and similar chromatographic retention times, optimization of the separation method is paramount. Without adequate peak separation, co-injection and comparison to standards will only reveal so much. After working on optimizing the chromatographic method, adequate separation of a mixture of 13 nitrogen heterocycles was achieved. This separation has two exceptions; co-elution of nitrogen heterocycles occurs in two separate peaks (uracil, 2,6-diaminopurine, and 6,8-diaminopurine around 28 min and adenine and xanthine around 32 min) in the standard nitrogen heterocycle chromatogram. **Figure 2.16** below represents the chromatograms of four standard nitrogen heterocycle solutions. The retention times of these standards are used for compound identification, and comparison of these chromatograms identified which compounds co-eluted.

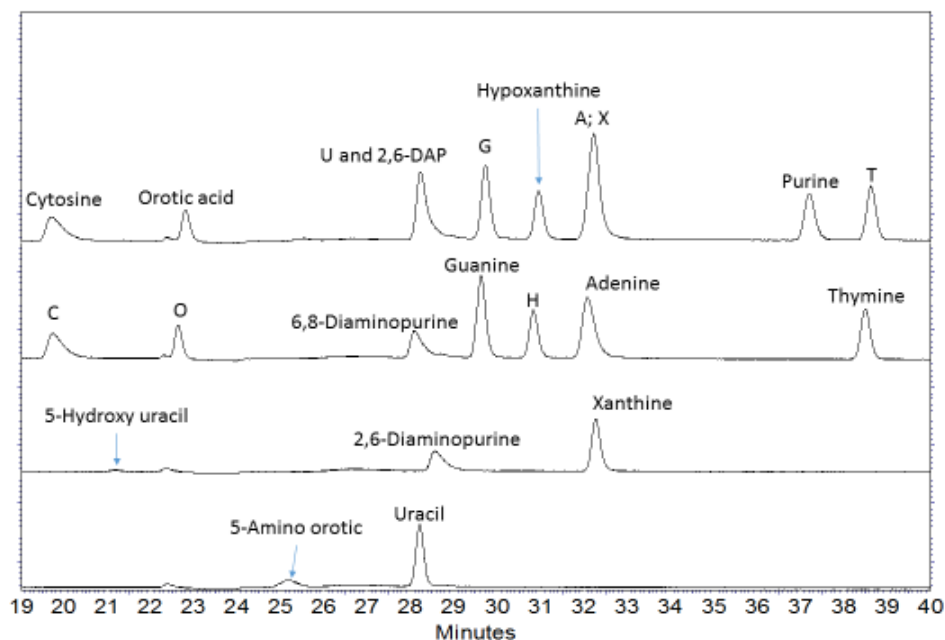


Figure 2.16. HPLC-UV chromatograms of four different mixtures of nitrogen heterocycle reference standards in 0.1 M NH_4OH . Peaks are labeled as follows: cytosine (C), 5-hydroxyuracil (5h), orotic acid (O), 5-aminoorotic acid (5ao), uracil (U), 2,6-diaminopurine (2,6-DAP), 6,8-diaminopurine (6,8-DAP), guanine (G), hypoxanthine (H), adenine (A), xanthine (X), purine (P), and thymine (T).

The retention time, including standard deviation, for reference nitrogen heterocycles are shown in **Table 2.4**. Some nitrogen heterocycles are weakly absorbing at 260 nm such as 5-hydroxyuracil and 5-aminoorotic acid, which increases their limit of detection. The peak for orotic acid at 22.65 ± 0.02 min is sharp but elutes at an aberrant location in the blank chromatogram of 0.1 M ammonium hydroxide. In this region, a small peak elutes adjacent to the peak associated with the orotic acid standard. This is not considered problematic as the peak of orotic acid is strong, sharp, and easily distinguished from the aberrant background peak.

Table 2.4. HPLC-UV retention times of nitrogen heterocycles. Abbreviations for compounds are shown in parentheses. Standard deviation (SD) has been shown in minutes (min.) and seconds (sec.).

Retention Times of Nitrogen heterocycles			
Nitrogen heterocycle	Average (min.)	SD (min.)	SD (sec.)
Cytosine (C)	19.75	0.01	0.89
5-hydroxyuracil (5hU)	21.15	0.01	0.35
Orotic acid (O)	22.65	0.02	0.97
5-aminoorotic acid (5aO)	25.14	0.01	0.64
6,8-diaminopurine (U)	28.12	0.03	2.08
Uracil (U)	28.18	0.04	2.53
2,6-diaminopurine (U)	28.57	0.01	0.73
Guanine (G)	29.66	0.04	2.28
Hypoxanthine (H)	30.87	0.04	2.30
Adenine (A)	32.13	0.04	2.48
Xanthine (A)	32.28	0.02	1.11
Purine (P)	37.11	0.08	4.80
Thymine (T)	38.54	0.04	2.38

In the following **Figures 2.17 – 2.22**, the nitrogen heterocycles that have been tracked through the different temperature series and time series reactions have been assigned specific labels. These labels are listed in **Table 2.4** and are as follows: cytosine (C), 5-hydroxyuracil (5hU), orotic acid (O), 5-aminoorotic acid (5aO), guanine (G), hypoxanthine (H), purine (P), and thymine (T). There are two peaks associated with co-eluting nitrogen heterocycles that need special acknowledgement, the peak associated with uracil, 2,6-diaminopurine, and 6,8-diaminopurine have all been assigned as (U) and the peak associated with adenine and xanthine is assigned as (A).

Nucleobases in the Time and Temperature Reaction Matrix

All five of the canonical nucleobases (cytosine, uracil, thymine, guanine, and adenine) commonly found in Earth's biosphere were determined in the supernatant using HPLC with UV detection at 260 nm. Cytosine was not detected above the instrument's

limit of detection (10 picomoles on column) throughout the entire time and temperature reactions. Analysis for uracil was more complicated due to peak co-elution with 2,6- and 6,8-diaminopurine. However, there was a peak that corresponds to the retention time of these compounds in multiple HPLC-UV chromatograms, most noticeable at the 200 °C reaction temperature. Thus, at least one of these compounds among uracil, 2,6- and 6,8-diaminopurine was likely produced in the 200 °C NH₄CN reactions. Thymine is difficult to discern. In multiple UV chromatograms, there is a peak near the thymine standard peak, which may be thymine. Interestingly, there is a very large peak near the retention time of thymine in the supernatant of the reaction conducted at 50 °C for 3 hours but this compound is likely not thymine because its lambda max is 295 nm (while thymine's lambda max is ~260 nm).

Best matches for guanine were found in the 50 and 200 °C NH₄CN reaction (both 3-hour reaction times). Also, there are peaks located within the standard deviation (0.04 min) of the retention time of guanine (29.66 min) in other reactions. Adenine and xanthine co-elute at almost the same retention time. There is a very closely associated peak to these standards in almost all supernatant samples. Furthermore, a distinct peak for the entire temperature series at 24 hours and 72 hours is easily observable. Adenine is typically the nucleobase synthesized in the highest abundance in cyanide reactions, so the presence of adenine here is not completely surprising. It's worth mentioning that both adenine and xanthine were identified as thermochemolysis-derived compounds of the cyanide polymer by GC-MS and comparison with the NIST mass spectral library. Therefore, we conclude that both adenine and xanthine are likely to be present in many of the supernatant samples.

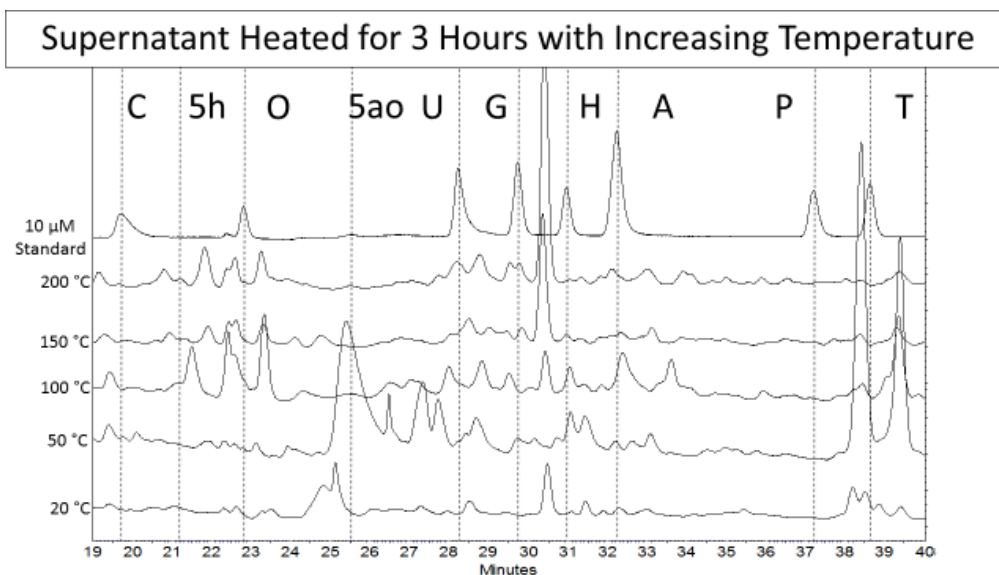


Figure 2.17. UV chromatograms of the supernatant isolated from NH_4CN reactions heated at different temperatures for 3 hours. 20 °C is a 6-month room temperature NH_4CN reaction. Compounds are cytosine (C), 5-hydroxyuracil (5h), orotic acid (O), 5-aminoorotic acid (5ao), uracil (U) co-elutes with 2,6 and 6,8-diaminopurine (2,6-DAP and 6,8-DAP), guanine (G), hypoxanthine (H), adenine (A) co-elutes with xanthine (X), purine (P), and thymine (T). Dashed lines are retention times of associated N-heterocycle standard peak.

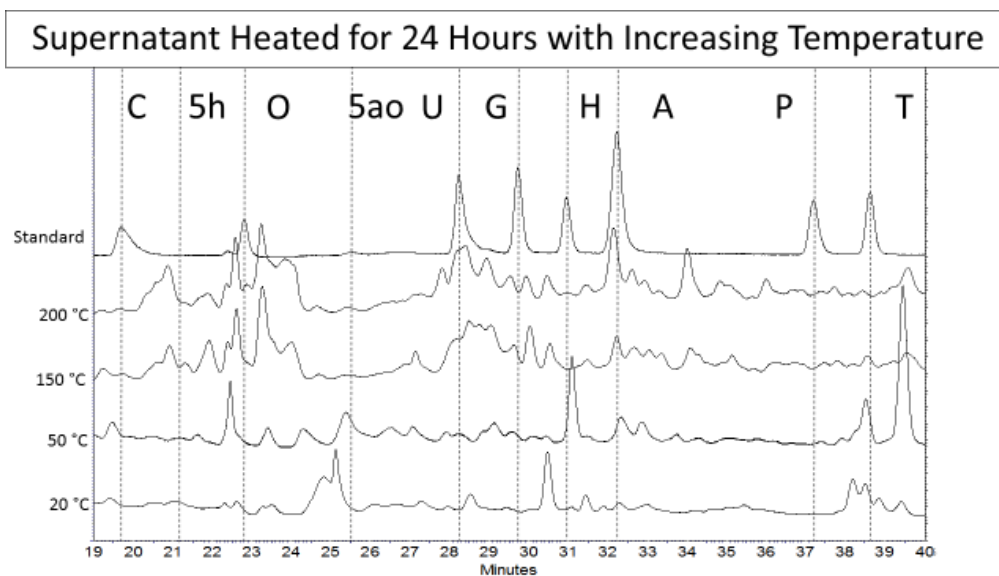


Figure 2.18. UV chromatograms of the supernatant isolated from NH_4CN reactions heated at different temperatures for 24 hours. 20 °C is a 6-month room temperature NH_4CN reaction. Compounds are cytosine (C), 5-hydroxyuracil (5h), orotic acid (O), 5-aminoorotic acid (5ao), uracil (U) co-elutes with 2,6 and 6,8-diaminopurine (2,6-DAP and 6,8-DAP), guanine (G), hypoxanthine (H), adenine (A) co-elutes with xanthine (X), purine (P), and thymine (T). Dashed lines are the retention times of associated N-heterocycle standard peak.

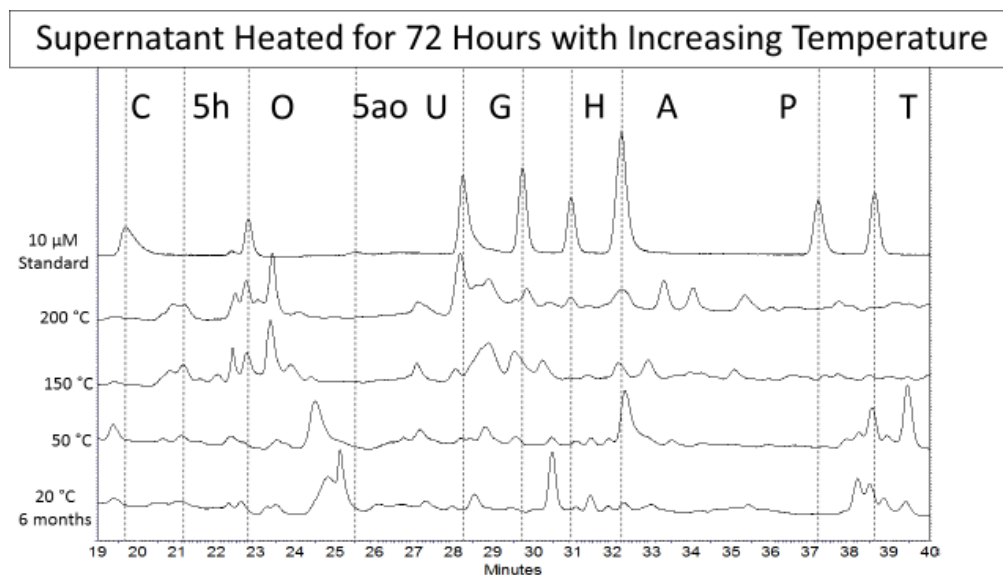


Figure 2.19. UV chromatograms of the supernatant isolated from NH_4CN reactions heated at different temperatures for 72 hours. 20 °C is a 6-month room temperature NH_4CN reaction. Compounds are cytosine (C), 5-hydroxyuracil (5h), orotic acid (O), 5-aminoorotic acid (5ao), uracil (U) co-elutes with 2,6 and 6,8-diaminopurine (2,6-DAP and 6,8-DAP), guanine (G), hypoxanthine (H), adenine (A) co-elutes with xanthine (X), purine (P), and thymine (T). Dashed lines are the retention times of associated N-heterocycle standard peak.

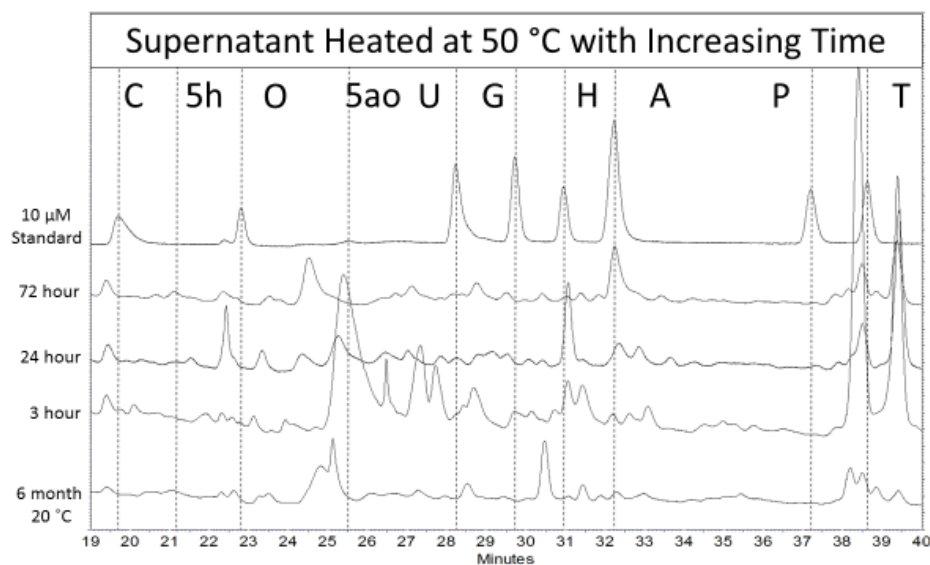


Figure 2.20. UV chromatograms of the supernatant isolated from NH_4CN reactions heated at 50 °C for different times. Also shown is the 6-month room temperature (20 °C) NH_4CN reaction. Compounds are cytosine (C), 5-hydroxyuracil (5h), orotic acid (O), 5-aminoorotic acid (5ao), uracil (U) co-elutes with 2,6 and 6,8-diaminopurine (2,6-DAP and 6,8-DAP), guanine (G), hypoxanthine (H), adenine (A) co-elutes with xanthine (X), purine (P), and thymine (T). Dashed lines are the retention times of associated N-heterocycle standard peak.

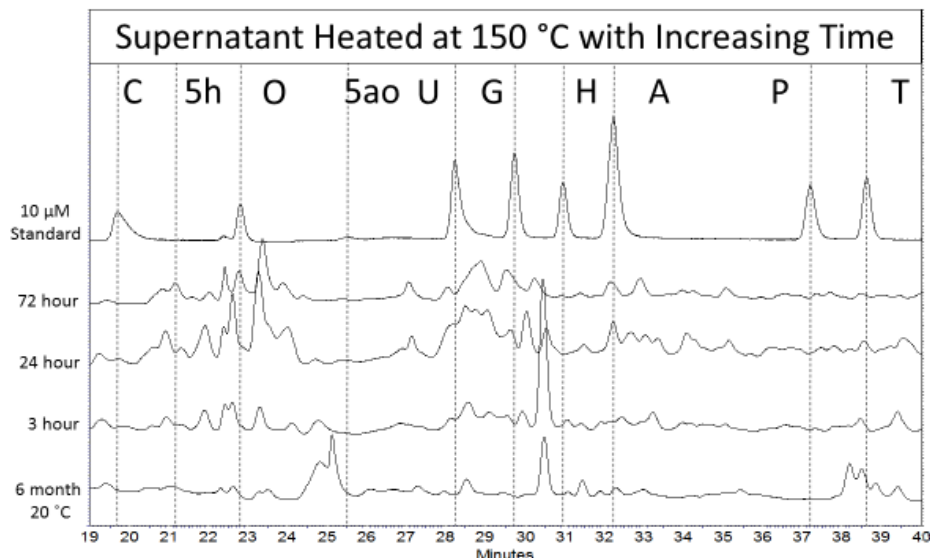


Figure 2.21. UV chromatograms of the supernatant isolated from NH_4CN reactions heated at $150\text{ }^\circ\text{C}$ for different times. Also shown is the 6-month room temperature ($20\text{ }^\circ\text{C}$) NH_4CN reaction. Compounds are cytosine (C), 5-hydroxyuracil (5h), orotic acid (O), 5-aminoorotic acid (5ao), uracil (U) co-elutes with 2,6 and 6,8-diaminopurine (2,6-DAP and 6,8-DAP), guanine (G), hypoxanthine (H), adenine (A) co-elutes with xanthine (X), purine (P), and thymine (T). Dashed lines are the retention times of associated N-heterocycle standard peak.

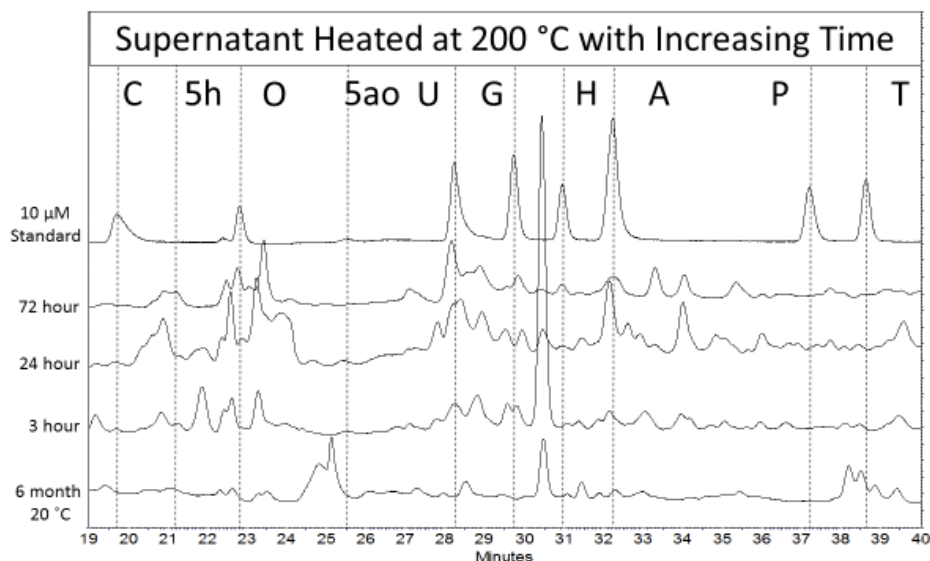


Figure 2.22. UV chromatograms of the supernatant isolated from NH_4CN reactions heated at $200\text{ }^\circ\text{C}$ for different times. Also shown is the 6-month room temperature ($20\text{ }^\circ\text{C}$) NH_4CN reaction. Compounds are cytosine (C), 5-hydroxyuracil (5h), orotic acid (O), 5-aminoorotic acid (5ao), uracil (U) which co-elutes with 2,6 and 6,8-diaminopurine (2,6-DAP and 6,8-DAP), guanine (G), hypoxanthine (H), adenine (A) co-elutes with xanthine (X), purine (P), and thymine (T). Dashed lines indicate the retention times of the associated N-heterocycle standard peak.

Remaining Nitrogen heterocycles in the Reaction Matrix

The nitrogen heterocycles 5-hydroxyuracil, orotic acid, 5-aminoorotic acid, 2,6-diaminopurine, 6,8-diaminopurine, hypoxanthine, xanthine, and purine were searched for in the supernatant portion of all reactions produced. The results for 2,6-diaminopurine and 6,8-diaminopurine as well as xanthine were discussed earlier since they co-elute with canonical nucleobases.

5-Hydroxyuracil may be present in the 72-hour temperature series based on the appearance of small peaks at the appropriate retention time; the strongest peaks appear to be in the 150 and 200 °C reactions (**Figure 2.19**). Also, note that there is not a peak for 5-hydroxyuracil in the reference standard solutions shown in **Figure 2.16 - 2.22**, only a dashed line to indicate the appropriate retention time. Since this nitrogen heterocycle has a very weak absorption at 260 nm, the observable peak indicates that 5-hydroxyuracil would be present in some significant amount. Orotic acid has similar behavior to 5-hydroxyuracil where the peak appears to get stronger in the 150 °C and 200 °C reactions at 72 hours. A very strong and broad peak corresponding to the retention time of 5-aminoorotic was observed in the 50 °C reaction at 3 hours and appears to decrease as the reaction proceeds; however, this compound is most likely not 5-aminoorotic since its UV spectrum differs from the reference standard. Hypoxanthine appears to be present in multiple reactions; however, the small peak appearance and slight retention time shifts make it difficult to determine. The best match for hypoxanthine was found in the 200 °C reaction at 72 hours. Some amount of hypoxanthine present may be due to deamination of adenine to hypoxanthine, which may occur at higher reaction temperatures. Purine does not have any significant peaks within the reaction matrix.

Table 2.5 represents whether these nitrogen heterocycles are present in the reaction matrix. With the color-coding employed, it seems that a higher number of nitrogen heterocycles were identified in the higher temperature, longer duration NH_4CN reactions. It's important to point out that this "yes" (green box) designation means these nitrogen heterocycles were more easily identified (by clear peaks centered around the correct retention times) and not necessarily that they were more abundant compared to other reactions. HPLC-UV identification of nitrogen heterocycles was considered tentative only due to the very complex nature of these samples. Two of the peaks observed in the standard solutions represent five different compounds. This must be considered when observing peaks in the supernatant; many of these peaks may represent absorbances of more than one compound. Recently, liquid chromatography-mass spectrometry (LC-MS) was used to analyze these supernatant samples, which provides unambiguous identification of nitrogen heterocycles by means of elemental composition and chromatographic retention time. This data will be incorporated into a manuscript for submission to a peer-reviewed science journal and is not presented here in this thesis. *Nevertheless, an important finding of this study was that multiple nitrogen heterocycles appear to be synthesized in high temperature NH_4CN reactions and recovered in the supernatant portion.*

Table 2.5. HPLC-UV determination of N-heterocycles present in the reaction matrix. (X) indicates times/temperatures not studied. Gray are reactions performed, but no supernatant was recovered. Green indicates supernatant peaks associated to retention time. Yellow indicates a peak is present, but outside the standard deviation of the retention time of a standard. Red indicates a peak was not detected.

Adenine / Xanthine					Hypoxanthine				
Temp (°C)	6 months	3 hrs	24 hrs	72 hrs	Temp (°C)	6 months	3 hrs	24 hrs	72 hrs
20	Yellow	X	X	X	20	Yellow	X	X	X
50	X	Green	Yellow	Yellow	50	X	Yellow	Yellow	Yellow
100	X	Yellow	Gray	Gray	100	X	Yellow	Gray	Gray
150	X	Red	Green	Green	150	X	Green	Red	Red
200	X	Yellow	Green	Green	200	X	Red	Yellow	Green

Guanine					Orotic Acid				
Temp (°C)	6 months	3 hrs	24 hrs	72 hrs	Temp (°C)	6 months	3 hrs	24 hrs	72 hrs
20	Red	X	X	X	20	Red	X	X	X
50	X	Green	Yellow	Yellow	50	X	Yellow	Red	Red
100	X	Red	Gray	Gray	100	X	Red	Gray	Gray
150	X	Yellow	Yellow	Yellow	150	X	Red	Red	Green
200	X	Green	Red	Yellow	200	X	Red	Yellow	Green

Uracil / 6,8- / 2,6-diaminopurine					5-hydroxyuracil				
Temp (°C)	6 months	3 hrs	24 hrs	72 hrs	Temp (°C)	6 months	3 hrs	24 hrs	72 hrs
20	Red	X	X	X	20	Red	X	X	X
50	X	Yellow	Yellow	Red	50	X	Red	Red	Green
100	X	Yellow	Gray	Gray	100	X	Yellow	Gray	Gray
150	X	Yellow	Yellow	Yellow	150	X	Red	Red	Green
200	X	Green	Yellow	Green	200	X	Yellow	Red	Green

Thymine					5-aminoorotic acid				
Temp (°C)	6 months	3 hrs	24 hrs	72 hrs	Temp (°C)	6 months	3 hrs	24 hrs	72 hrs
20	Yellow	X	X	X	20	Red	X	X	X
50	X	Yellow	Yellow	Green	50	X	Yellow	Yellow	Red
100	X	Yellow	Gray	Gray	100	X	Red	Gray	Gray
150	X	Yellow	Yellow	Red	150	X	Red	Red	Red
200	X	Red	Red	Red	200	X	Red	Red	Red

Cytosine					Purine				
Temp (°C)	6 months	3 hrs	24 hrs	72 hrs	Temp (°C)	6 months	3 hrs	24 hrs	72 hrs
20	Red	X	X	X	20	Red	X	X	X
50	X	Red	Red	Red	50	X	Red	Red	Red
100	X	Red	Gray	Gray	100	X	Red	Gray	Gray
150	X	Red	Yellow	Red	150	X	Red	Red	Red
200	X	Red	Red	Red	200	X	Red	Red	Red

N-Heterocycle Present			
Yes	Maybe	No	
X indicates a reaction time/temperature not performed			
Reaction performed, no supernatant was produced			

Conclusion

This study was meant to model cyanide chemistry thought to have occurred in some meteorite parent bodies. Novel aspects included a temperature study of NH_4CN reactions and focus on the synthesis and survivability of nucleobases and nitrogen heterocycles in both the liquid supernatant and solid polymer of a reaction mixture.

Herein, it has been determined that heating aqueous NH_4CN reactions (hydrothermal cyanide chemistry) induces significant changes in the bulk properties of both the supernatant and polymer as shown by ATR-FTIR spectroscopy. Further analysis of the polymer by TMAH-GC-MS detected the presence of many nitrogen heterocycles. Adenine, hypoxanthine, xanthine, and cyanuric acid were identified with good to excellent matches to the NIST 2014 MS database. The data showed a clear correlation between compound abundance and NH_4CN reaction temperature. Nitrogen containing compound abundances (including nitrogen heterocycles) decrease with increasing NH_4CN reaction temperature. An opposite correlation is observed when analyzing the aromatic compound production, where these products increase in abundance with increasing NH_4CN reaction temperature.

NH_4CN polymer has been considered a “safe haven” for the long-term storage of nitrogen heterocycles during periods of intense heating and/or radiation. The results obtained from TMAH GC-MS suggest that increases in reaction temperature alter the structure of the cyanide (hetero)polymer and that the nitrogen heterocyclic character is reduced in favor of a more aromatic character. NH_4CN polymer may still be considered a reservoir to contain biologically relevant compounds for later release in a primordial environment; however, its effectiveness may be diminished depending on the initial reaction conditions, particularly increased temperature.

Finally, HPLC analysis of the supernatant shows a similar trend. There are peaks closely associated to the retention times within the standard nitrogen heterocycle mixtures. These peaks correspond to reported products of NH_4CN reactions. Nitrogen heterocycle production continues with increasing temperature, but one must be careful while

interpreting this data as compound identification using HPLC-UV was tentative and ambiguous. The composition of the supernatant is complex. HPLC-UV chromatograms of the supernatant show many peaks representing many compounds. The majority of these compounds remain unidentified. Several of these unknown peaks increase with increasing NH_4CN reaction temperature, while several other unknown peaks decrease with increasing NH_4CN reaction temperature. What can be determined is that these unknown peaks are UV-absorbing compounds (chromophores) that are likely aromatic or heterocyclic in nature. Adenine, hypoxanthine, and xanthine are likely to be produced in these temperature series reactions. The HPLC-UV findings correlate well with the thermochemolysis analysis of the polymer which identified aromatic and heterocyclic compounds with good to excellent matches to the NIST MS database. The observed production of several compounds present in the supernatant increases with reaction temperature. Concurrent studies of these products by LC-MS are needed for unambiguous identification and quantitation of the nitrogen heterocycles studied in this thesis.

Nitrogen heterocycles found in this study correlate well to literature reporting purine nitrogen heterocycles in aqueously altered CI and CM carbonaceous chondrites (meteorites), which have experienced a similar temperature range on the parent body. Furthermore, low abundance of nitrogen heterocycles in CI chondrites may be explained by their greater degree of thermal and aqueous alteration, which was consistent with the lower production of nitrogen heterocycles observed in the polymer of heated cyanide reactions.

CHAPTER THREE: GAMMA RADIOLYSIS OF NITROGEN HETEROCYCLES

Introduction

Asteroids contain primitive organic material, which has been partly characterized through the laboratory analysis of meteorites.⁴⁸ While this extraterrestrial material has not been processed extensively from the time of Solar System formation, radionuclide decay within asteroids has played an important role in processing this organic material over the last 4.568 billion years (the age of the Solar System).¹ Radioactive decay of elements causes heating, but may also have other effects on the chemical nature of these compounds.⁴⁹ Since intact nitrogen heterocycles are found in meteorites, we performed a radiolysis study in order to understand the effects of prolonged radiation exposure and possibly extrapolate the distribution and abundance of nitrogen heterocycles to 4 billion years ago, which corresponds to the proposed Late Heavy Bombardment period (when a very large number of asteroids struck the early Earth).³²

Studies have shown that asteroids have received ~14 MGy of radiation over the last 4.568 billion years and the majority of this radiation (11 MGy) was received in the first tens of millions of years of our Solar System's history.^{41, 42, 50, 51} Much of this radiation is experienced in the form of ~1.8 MeV gamma rays from the decay of aluminum-26 (²⁶Al). ²⁶Al has a cosmically short half-life of $\sim 7.1 \times 10^5$ years. After 10 half-lives (~7 million years), much of the initial amounts of this radionuclide have decayed to ²⁶Mg.⁵⁰⁻⁵² Cosmic rays and solar winds are prevalent, but are not considered deeply penetrating, only irradiating the surface to a depth of a few meters (<20 m). This leaves the remaining

majority of cosmic organics unperturbed by cosmic rays and left to the effects of gamma irradiation from other long-lived radionuclides present in the asteroids.⁵³

Many studies have been performed to investigate how organic compounds have formed and survived in a (simulated) harsh cosmic environment.⁵⁴⁻⁵⁸ Most of these studies focus on the effect that ionizing radiation has on the chirality of amino acids. These studies provide data explaining the non-racemic mixtures of amino acids observed in meteorites.⁵⁹ In this study, nitrogen heterocycles were exposed to a ⁶⁰Co source that releases a gamma photon of ~1.3 MeV.⁵² The effects of total dose and dose rate were investigated to gather an understanding of nitrogen heterocycle irradiative decomposition. Data gathered from these experiments will help in extrapolating abundances observed in modern meteorite analyses to the abundances of biologically relevant compounds present in asteroids during prebiotic times.

Experimental Methods

Materials

All glassware used in these experiments was wrapped in aluminum foil and baked out at 500 °C for 24 hours. Adenine >99%, guanine > 98%, and xanthine were purchased from Sigma-Aldrich. Acetic acid, purine, hypoxanthine, and 2,6-diaminopurine were purchased from Acros Organics. 8-aminoadenine (6,8-diaminopurine) was purchased from Tocris Bioscience. Ammonium hydroxide (NH₄OH) and HPLC grade acetonitrile were purchased from Fisher Chemical. All stock solutions were made using 18.2 MΩ·cm water (referred to as nanopure water) produced by a Barnstead Nanopure Diamond water purifier. Nitrogen heterocycles were dissolved in 0.1 M HPLC grade ammonium hydroxide to produce ~3 mM stock nitrogen heterocycle solutions. A serial dilution was then performed

to prepare (1, 10, 50, and 100 μM) standard solutions. Calibration curves for each nitrogen heterocycle were recorded. For liquid chromatographic separation, ammonium acetate buffer was prepared via NH_4OH titration of 20 mM acetic acid solution to pH 4.51. All reagents used for making the buffer solutions were HPLC grade and not filtered.

Sample Preparation

Nitrogen heterocycles are sparingly soluble in water. As a result, stock solutions of seven nitrogen heterocycles were prepared with 0.1 M NH_4OH as follows: adenine 4.7 mM, guanine 2.7 mM, xanthine 3.2 mM, hypoxanthine 4.9 mM, purine 3.6 mM, 2,6-diaminopurine 4.6 mM, and 8-aminoadenine 3.3 mM. 400 μL of stock solution was added to individual glass ampoules and heated to dryness at 60 $^\circ\text{C}$. Once dry, these ampoules were vacuum sealed on a glass Schlenk line using a hand-held butane torch. For each purine, 11 ampoules were prepared (4 non-irradiated controls and 7 samples for radiolysis). The ampoules were placed at a distance of 30 cm from a ^{60}Co γ -radiation source in order to receive a dose rate of ~ 350 Gy/hr. Seven ampoules for each heterocycle were placed around the γ -radiation source and removed from the source at 17 day time intervals in order to receive increasing doses of radiation (see **Table 3.1** and **Figure 3.1**). Maximum total dose was ~ 0.992 MGy, which took 119 days to complete. It was not scientifically feasible to perform studies on the order of 14 MGy (corresponding to radiation received by asteroids over 4.568 billion years), which couldn't be completed in the *normal* timeframe of a master's degree. Additionally, the canonical purines (six ampoules for guanine and five ampoules for adenine) were placed at varying distances from the radiation source in order to receive a total dose of ~ 250 kGy at increasing dose rates (see **Table 3.2** and **Figure 3.1**). Dose rate can be thought of as time of irradiation on the γ -source; therefore, a slower

dose rate means longer time on the source in order for the samples to receive the same total dose (~250 kGy).

Table 3.1. Total dose versus time data. Seven sample sets were placed at 30 cm from ^{60}Co source to receive a dose rate of ~350 Gy/hr. Sample sets were removed from the source in 17 day intervals. The last set was removed after 119 days and received 992 kGy of total dose.

Total Dose Received vs. Time			
Sample Set	Days	Hours	Total Dose (Gy)
1	17	408	141,739
2	34	816	283,478
3	51	1,224	425,218
4	68	1,632	566,957
5	85	2,040	708,696
6	102	2,448	850,435
7	119	2,856	992,174

Table 3.2. Dose rate versus time data. Six sample sets were placed at increasing distance from the ^{60}Co source to receive a total dose of 250 kGy at varying dose rates. Samples were removed from the radiation source in 17 day intervals. The last sample was removed after 119 days receiving a dose rate of ~87 Gy/hr.

Dose Rate Data					
Sample Set	Days	Hours	Distance (cm)	Dose Rate (Gy/h)	Total Dose (Gy)
1	34	816	32	304	241,252
2	51	1,224	39	207	249,533
3	68	1,632	45.5	154	249,043
4	85	2,040	51	123	251,225
5	102	2,448	56	103	252,886
6	119	2,856	61	87	251,236

To prepare samples for HPLC analysis, sealed ampoules were cracked open using disposable ampoule openers (Fisherbrand SafeSnap). A popping sound was observed upon opening ampoules for the majority of samples, which indicated that the vacuum seal had not been compromised. 400 μL 0.1 M NH_4OH was placed inside each ampoule and mixed

using a vortex mixer on low setting for 30 seconds. The ampoules were then allowed to rest for 20 minutes to dissolve the individual nitrogen heterocycle into solution. 200 μL sample solution (half of the volume already inside of the ampoule) was used to rinse the inside of the ampoule if material was stuck on the side of the ampoule. The 400 μL sample solution was transferred to an HPLC vial. An additional 400 μL 0.1 M NH_4OH was added to the ampoule and the process was repeated: vortex mixing, resting for 20 minutes, rinsing the sides, and sample solution transfer. A final volume of 200 μL was added and the procedure was performed one last time. This provided a 1 mL total volume of analyte solution for quantitative transfer of nitrogen heterocycles for HPLC analysis. A 100-fold dilution (10 μL of analyte was diluted into 990 μL of 0.1 M NH_4OH) for purines was performed for accurate quantitation using a standard concentration curve. Guanine does not readily dissolve in 0.1 M NH_4OH . Therefore, guanine samples were dissolved in 1 M NH_4OH and followed a slightly modified procedure to the above samples. Two 400 μL and one 200 μL aliquots of 1 M NH_4OH were performed as outlined above. After this, 9 successive 1 mL volumes were used to quantitatively rinse the ampoules for sample transfer into a 25 mL glass vial. From this 10 mL guanine solution, 100 μL guanine solution was diluted in 900 μL water in an HPLC vial, which results in the same 100-fold dilution as described earlier. Sample solutions were analyzed immediately by the HPLC instrument.

High Performance Liquid Chromatography

Irradiated samples, non-irradiated controls, and standard solutions were analyzed using a Thermo Scientific Accela high performance liquid chromatograph (HPLC) coupled to an Accela photodiode array UV-Vis detector (PDA). Nitrogen heterocycle separation was achieved by injecting 10 μL of sample or standard solution onto a Phenomenex

Synergi 4 μ Fusion reverse phase column (2 mm \times 150 mm; 80 angstrom pore size). The column temperature was maintained at 30 °C. Mobile phase A was composed of 20 mM ammonium acetate buffer at pH 4.51 and mobile phase B was 100% acetonitrile.

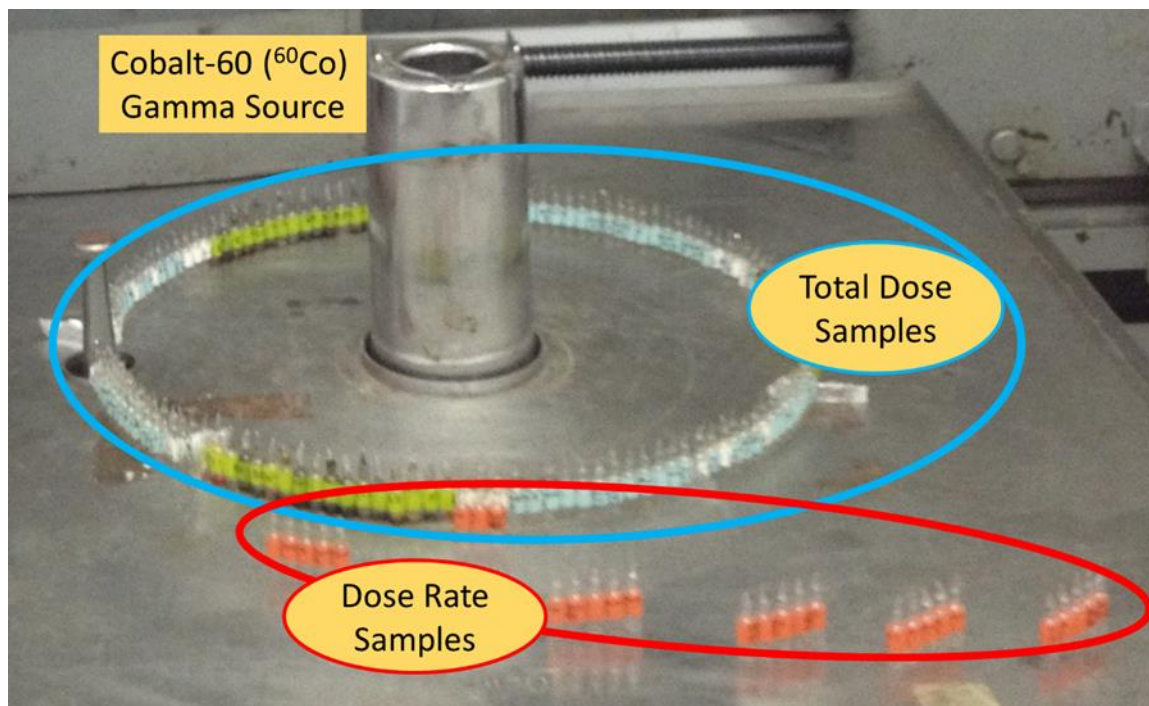


Figure 3.1. Radiolysis sample placement at the ^{60}Co source. Samples consist of nitrogen heterocycles vacuum sealed in glass ampoules and specifically placed for two separate analyses: total dose (blue/green) and dose rate (red). Gamma Radiation Facility, Tokyo Institute of Technology in Japan.

Samples and standards were eluted at 200 $\mu\text{L}/\text{min}$. using the following gradient: 0-10 min. 0-45% B, 10-12 min. 45-100% B, 12-17 min. 100% B, 17-19 min. 100-0% B, and 19-29 min. 0% B (flush and equilibration of column). Samples and standards were injected three separate times for triplicate analyses. The PDA detector recorded the UV spectrum from 200-400 nm. For nitrogen heterocycle analysis, the wavelength of 260 nm was typically monitored.

Results and Discussion

In this study, seven purine nitrogen heterocycles (**Figure 3.2**) were analyzed in order to investigate their stability and the potential degradation trends that may occur while exposed to γ -radiation. These nitrogen heterocycles were chosen because they have been previously identified in the formic acid extracts of carbonaceous chondrites, which are meteorites left over from the formation of the Solar System that contain significant amounts of organic compounds.²⁴ The abundance and distribution of these organic compounds do not likely reflect those originally present ~4.5 billion years ago when carbonaceous chondrite meteorites were delivered to the prebiotic Earth. The reason for these differences may be due to radiolysis in carbonaceous chondrite parent bodies that occurred over their entire lifetimes which likely altered the original abundance and distribution of organic compounds, including nitrogen heterocycles.^{41, 42} Therefore, we investigated how purine nitrogen heterocycles may have changed over time due to γ -radiation.

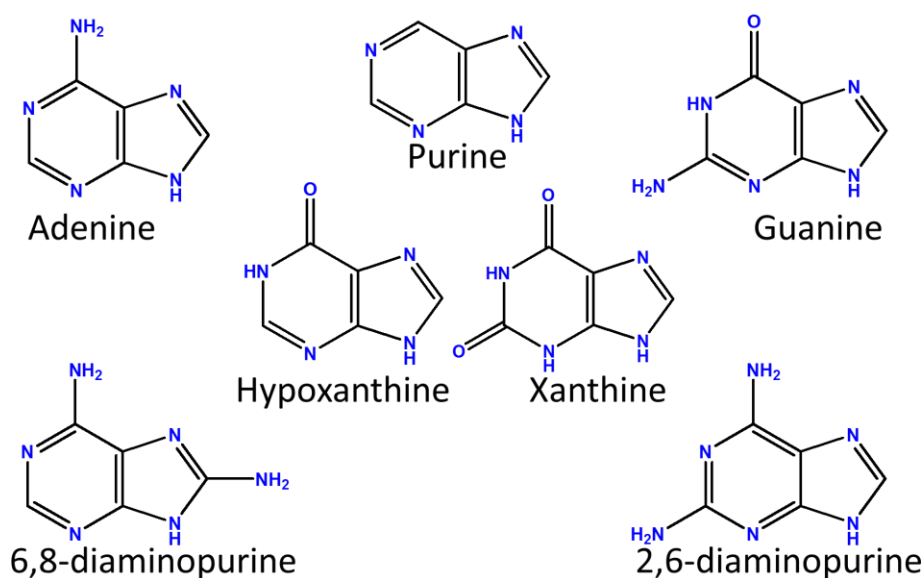


Figure 3.2. Purine nitrogen heterocycles investigated in the γ -irradiation studies. The purines selected for this analysis have been identified in formic acid extracts of meteorites and are produced in room temperature NH_4CN reactions.

Four-point calibration curves were generated for all purine nitrogen heterocycles using standard solutions with a concentration range of 1-100 μM (see **Figures 3.3 – 3.9**). All calibration curves were linear with goodness of fit $R^2 > 0.997$ within the region of analysis (2 orders of magnitude), which allowed for accurate quantitation of these compounds using the integrated peak areas.

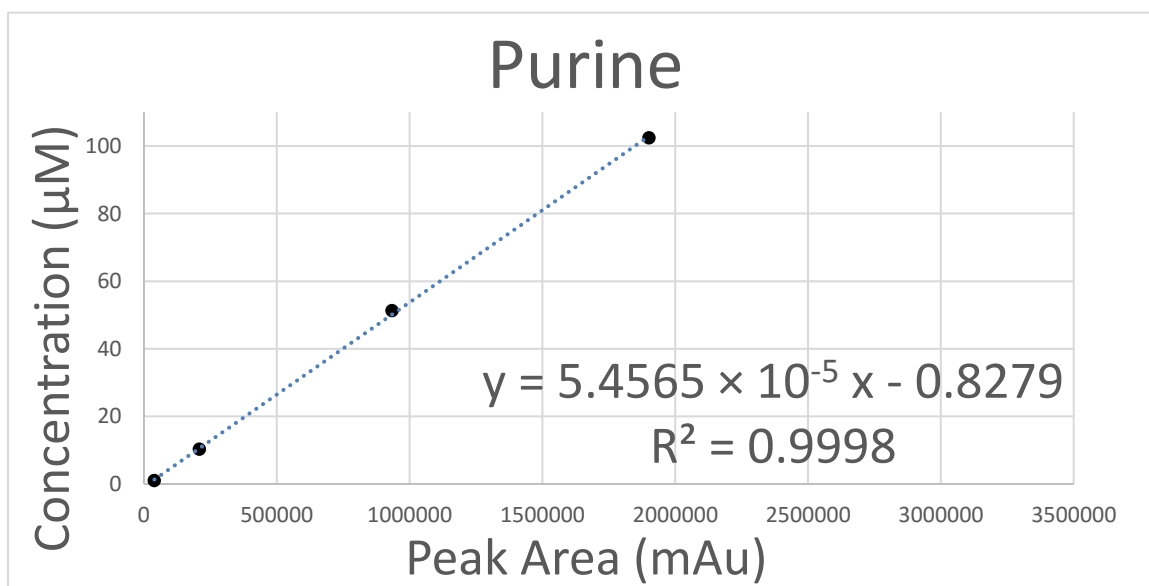


Figure 3.3. Purine calibration curve.

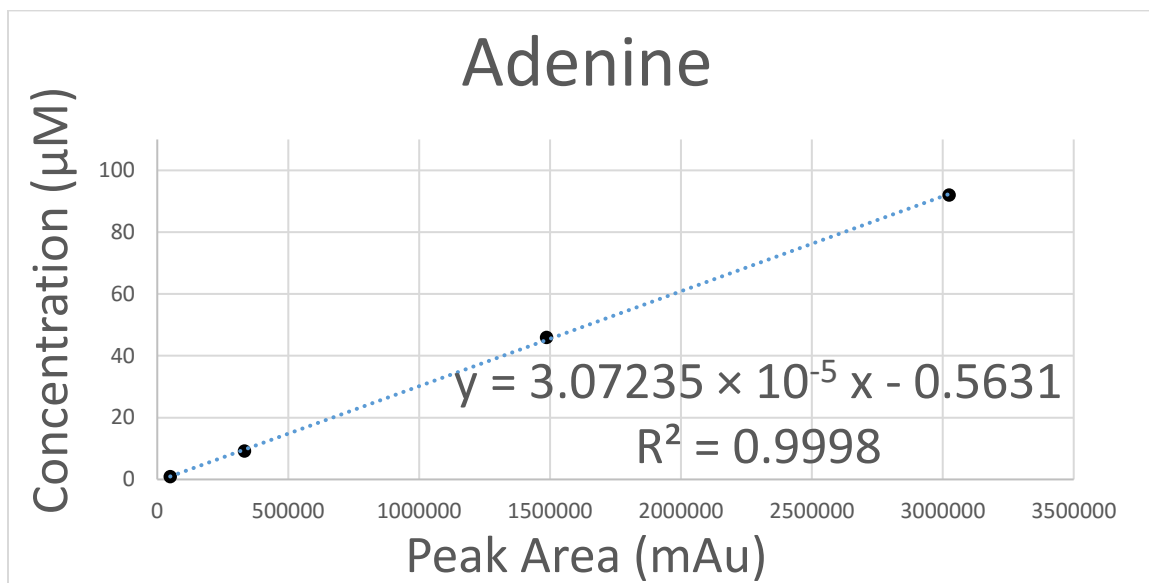


Figure 3.4. Adenine calibration curve.

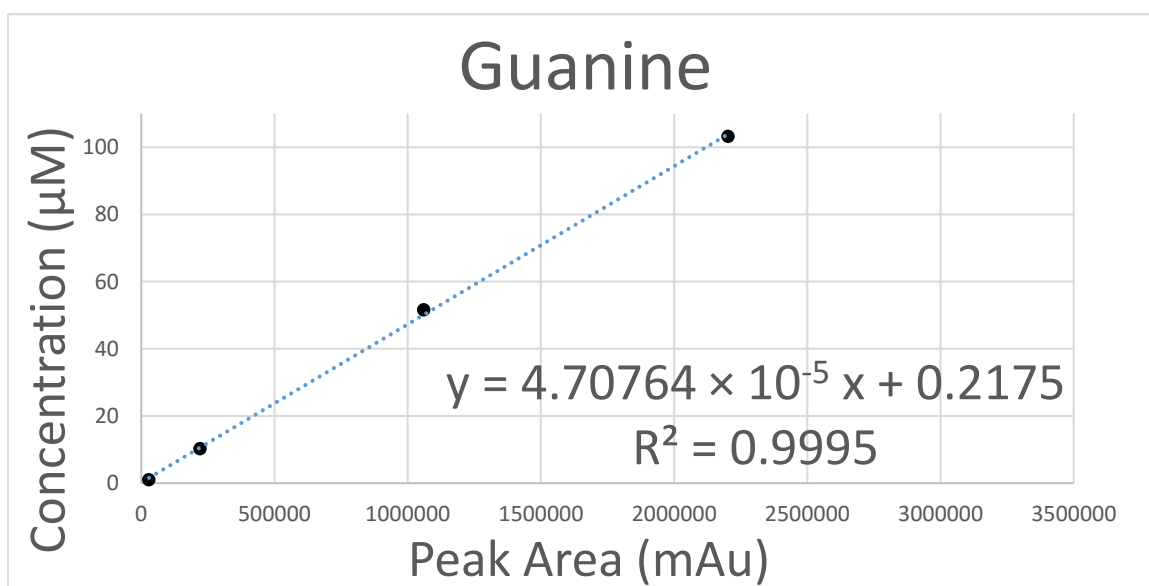


Figure 3.5. Guanine calibration curve.

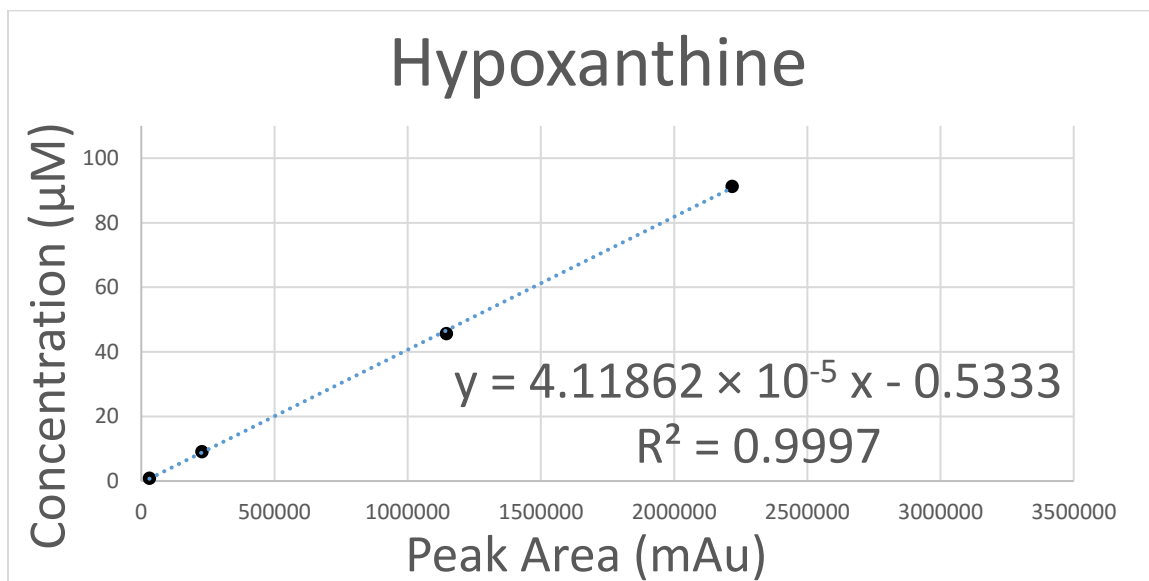


Figure 3.6. Hypoxanthine calibration curve.

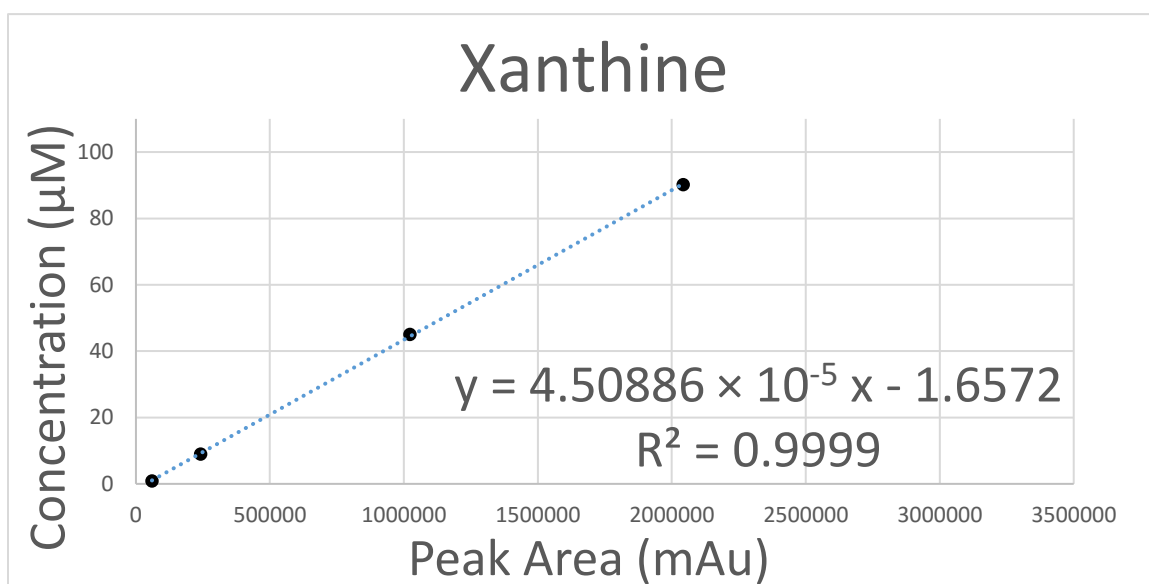


Figure 3.7. Xanthine calibration curve.

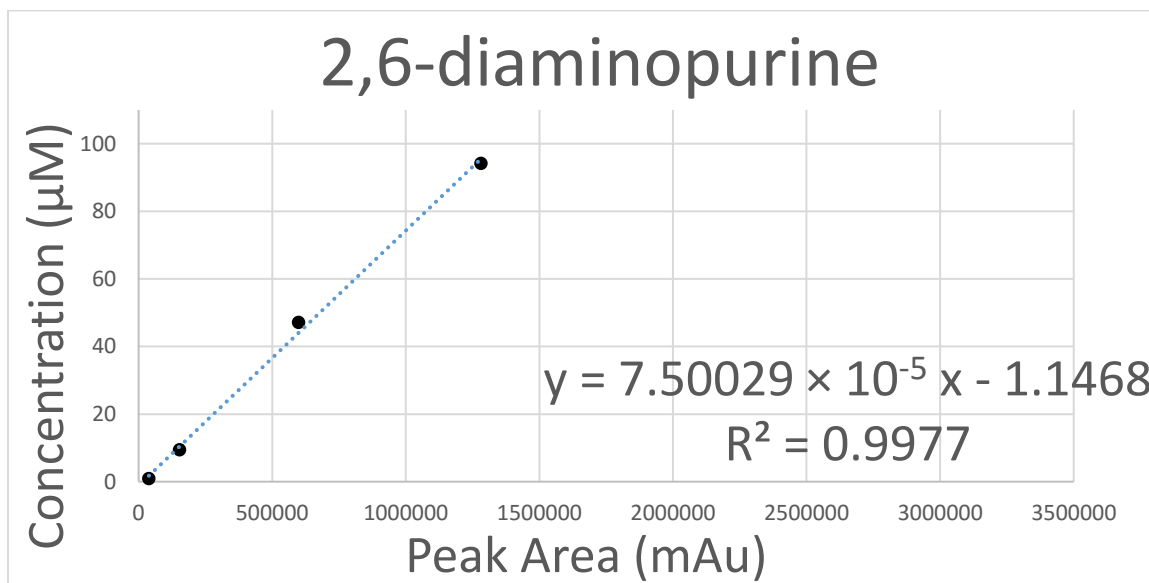


Figure 3.8. 2,6-diaminopurine calibration curve.

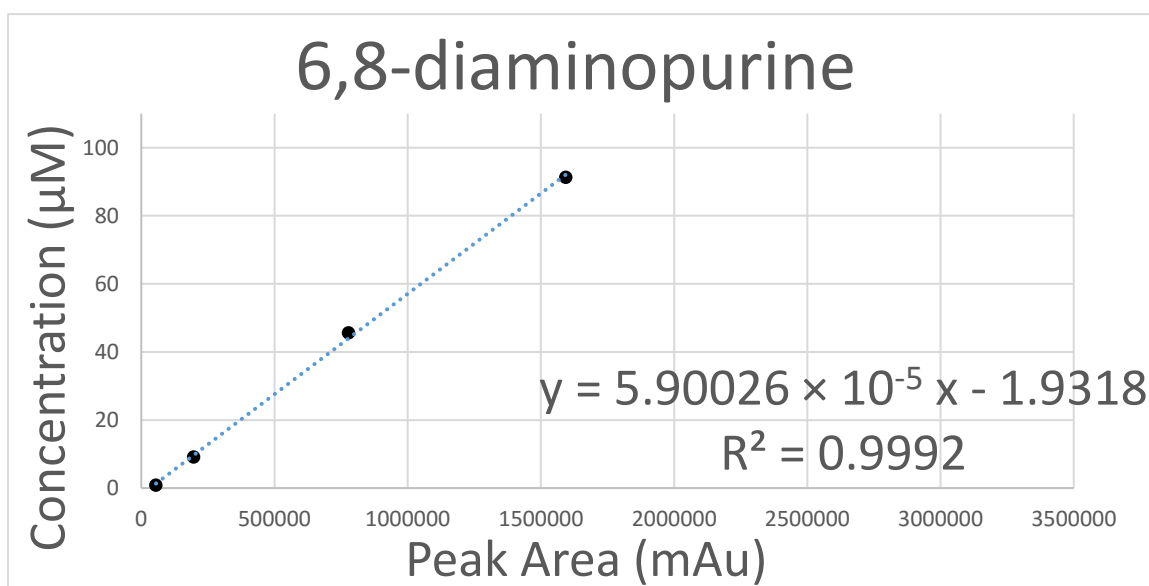


Figure 3.9. 6,8-diaminopurine calibration curve.

Two studies were performed in order to evaluate the radiolytic stability of nitrogen heterocycles: a total dose study and a dose rate study. For both studies, only one peak was detected in the UV chromatogram (corresponding to the respective parent nitrogen

heterocycle) for all seven purines. The percent recovery of the irradiated nitrogen heterocycles was initially calculated in two ways based on (1) integrated peak area (Equation 1) and (2) the mole ratio using the calibration curves (Equation 2).

$$\text{Area \%} = \frac{\text{Area (Irradiated Sample)}}{\text{Area (Unirradiated Control)}} \times 100 \quad \text{Eq. 1}$$

$$\text{Mole Ratio} = \frac{\text{Moles (Irradiated Sample)}}{\text{Moles (Unirradiated Control)}} \quad \text{Eq. 2}$$

However, when these data were plotted against the increasing total radiation dose or dose rate, the trend was the same (see data plotted for purine in **Figure 3.10** for an example of total dose data) and the choice was made to report data as percent recovery based on the integrated peak area for both studies.

The first study performed was a total dose study on the seven nitrogen heterocycles in order to evaluate their radiolytic stability with increasing total dose (up to 0.992 Megagrey (MGy) at a constant dose rate (~350 kGy/hr). **Figures 3.10-3.16** show the percent recovery vs. increasing total radiation dose for all of the irradiated nitrogen heterocycles (note that the data points at 0 Gy represent four non-irradiated control samples which were made at the same time and underwent the same preparation as all of the other samples). These plots show that these nitrogen heterocycles in the solid state display a resistance to decomposition from γ -radiation.

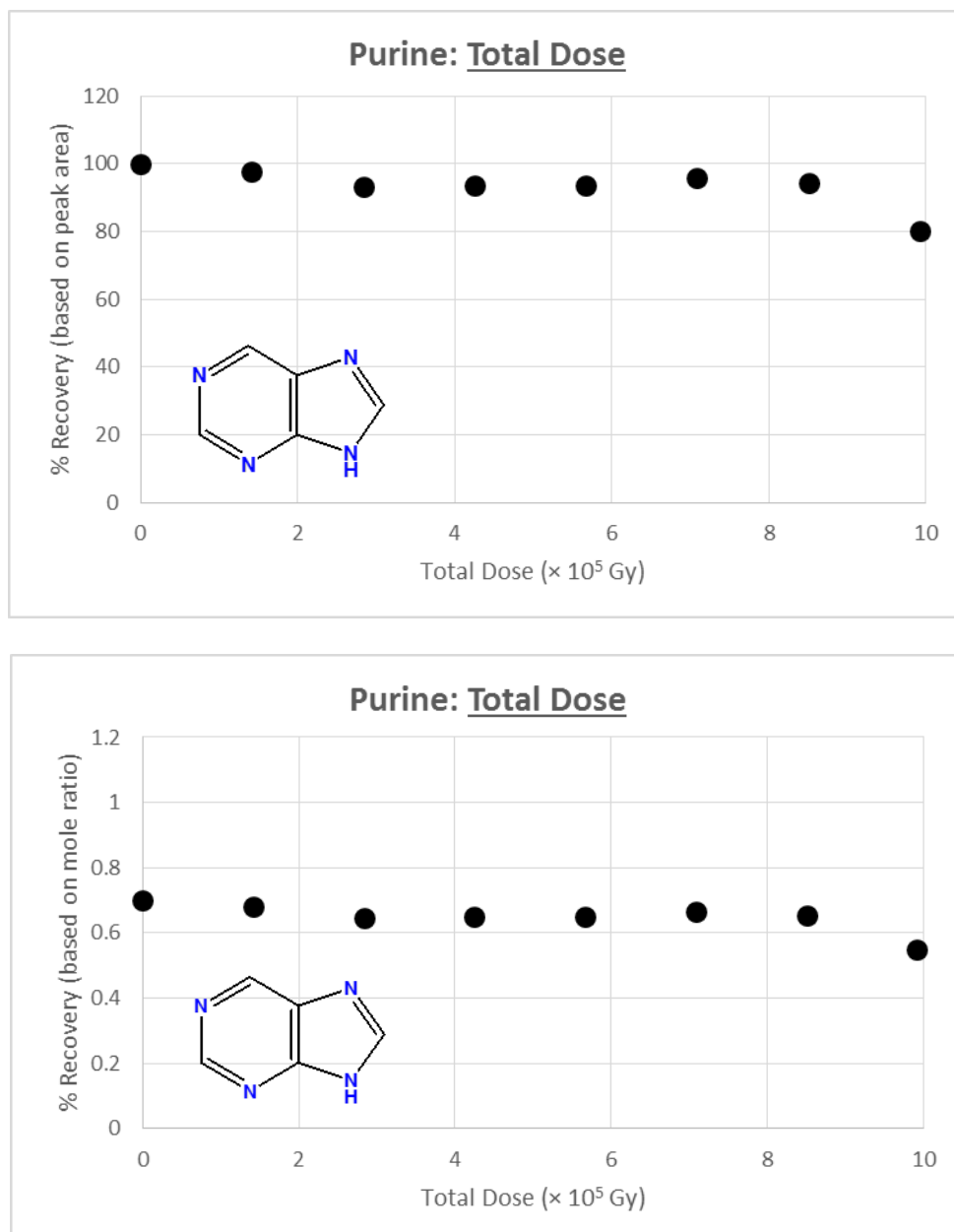


Figure 3.10. Total dose decay curve for purine. Decay curves are in terms of percent recovery based on peak area (top) and mole ratio (bottom). All further plots show percent recovery based on peak area. Purine undergoes 20 ± 3 % decomposition over the course of ~ 1 MGy of γ -radiation exposure. The majority of this decomposition occurs at higher doses (>800 kGy).

No degradation products were detected in UV chromatograms at 260 nm (or in the full spectrum scan from 200-400 nm). In the solid state, purines are remarkably stable with a maximum degradation of 53 % for guanine at radiation doses up to nearly 1 MGy of total

dose, as compared to the non-irradiated control (see **Table 3.3**). Virtually no degradation occurred in adenine and hypoxanthine. Xanthine remained nearly stable with the exception of the last data point showing a 29 % decrease, compared to the control. Xanthine's radiolytic stability is consistent with other methylated xanthines (theobromine, theophylline, and caffeine), although the latter studies used an electron beam (9.96 MeV) and doses to only 400 kGy.⁶⁰

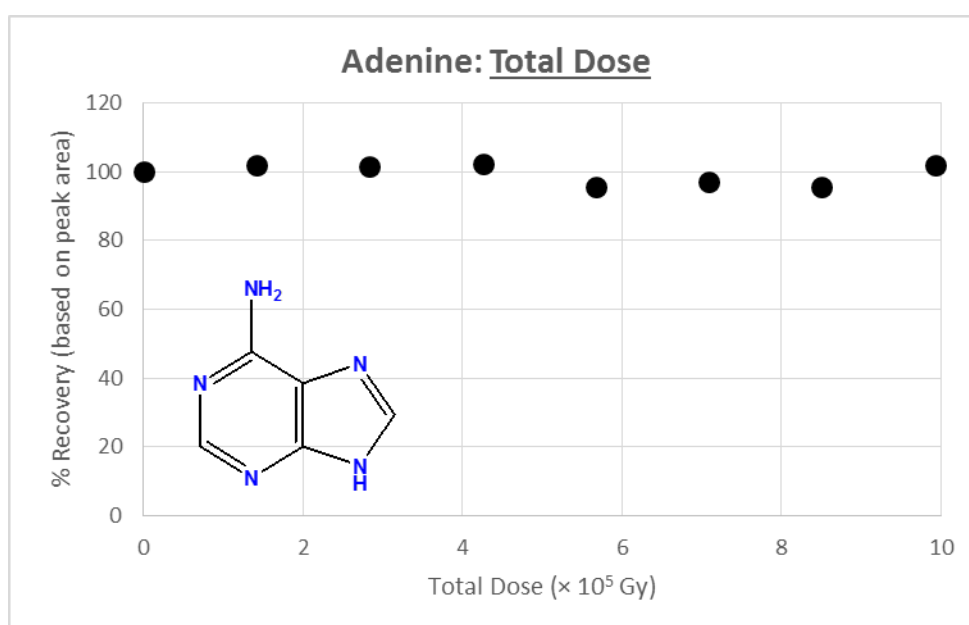


Figure 3.11. Total dose decay curve for adenine. Adenine was determined to have no discernable decomposition over the course of ~1 MGy of γ -radiation exposure.

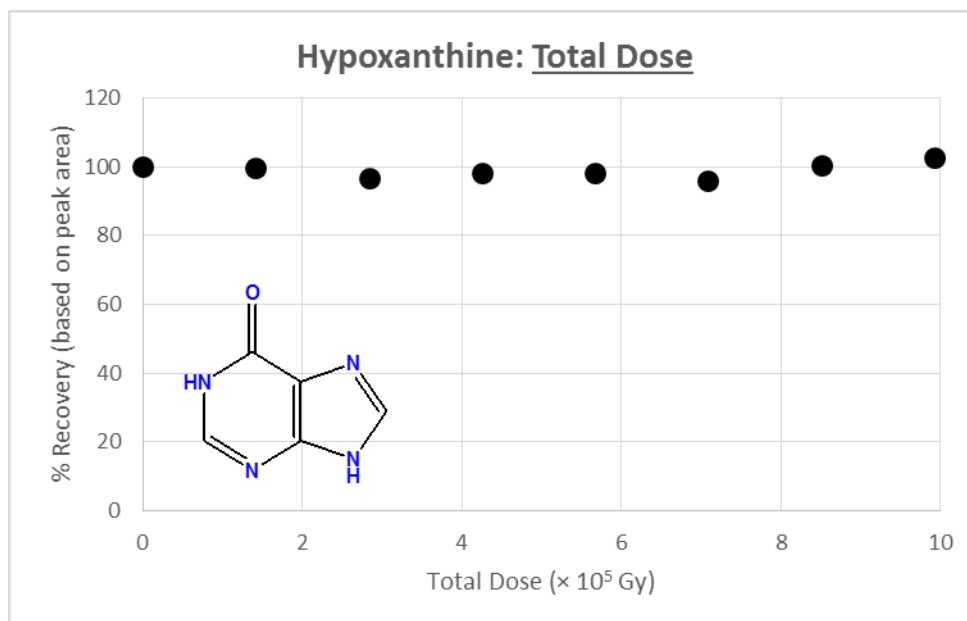


Figure 3.12. Total dose decay curve for hypoxanthine. Hypoxanthine is a deamination product of adenine. This replaces adenine's amine group with hypoxanthine's carbonyl group at the 6-position. Both adenine and hypoxanthine revealed no discernable decomposition over the course of ~1 MGy of γ -radiation exposure.

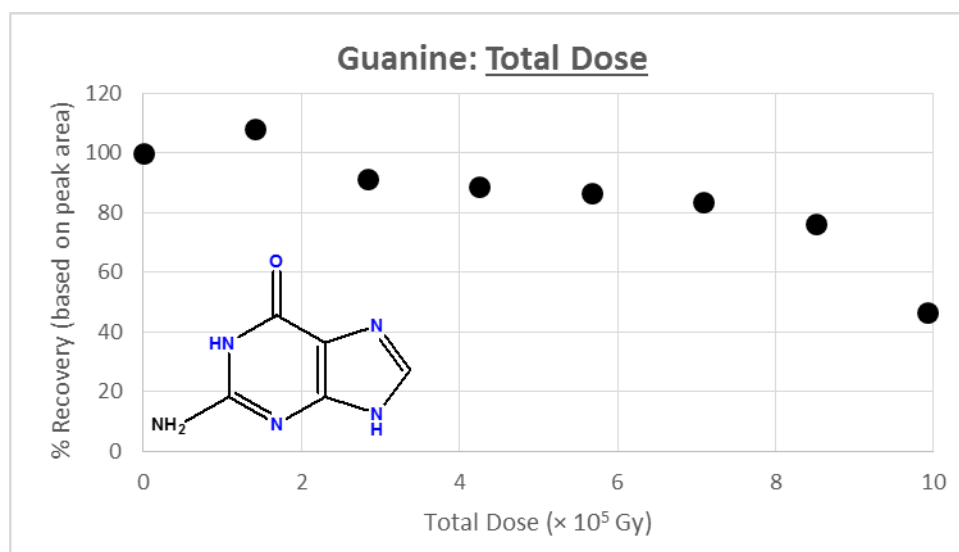


Figure 3.13. Total dose decay curve for guanine. Guanine gradually decomposes 53 ± 3 % of the initial amount over the course of ~1 MGy γ -radiation exposure. A large fraction of this loss occurs at high doses (>800 kGy).

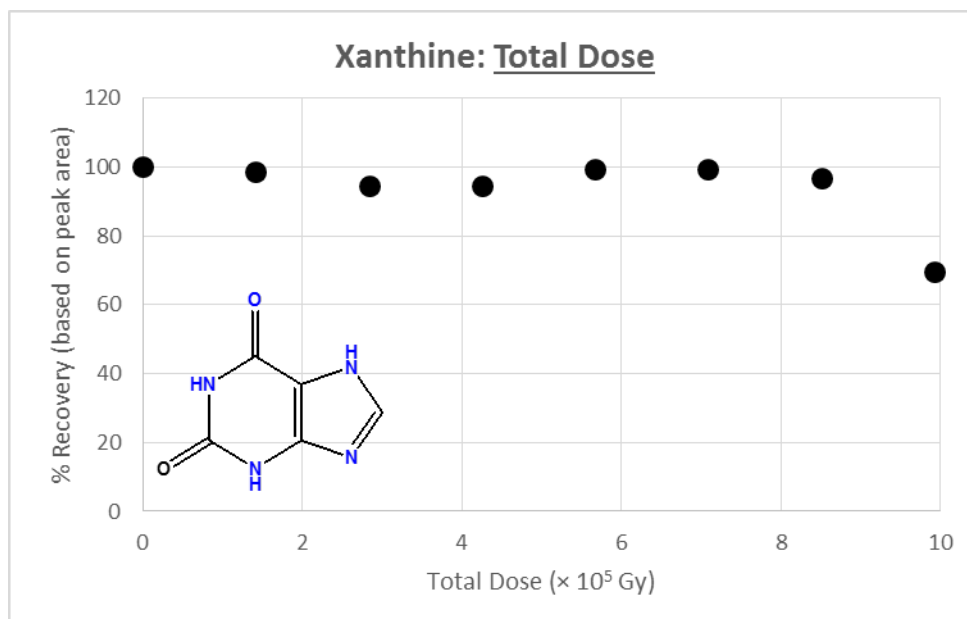


Figure 3.14. Total dose decay curve for xanthine. Xanthine is the deamination product of guanine. Replacement of an amine with carbonyl at the 2-position appears to provide radiolytic stability. Xanthine decomposes by 29 ± 3 % over the course of nearly 1 MGy γ -radiation exposure; most of which occurs after 800 kGy of exposure.

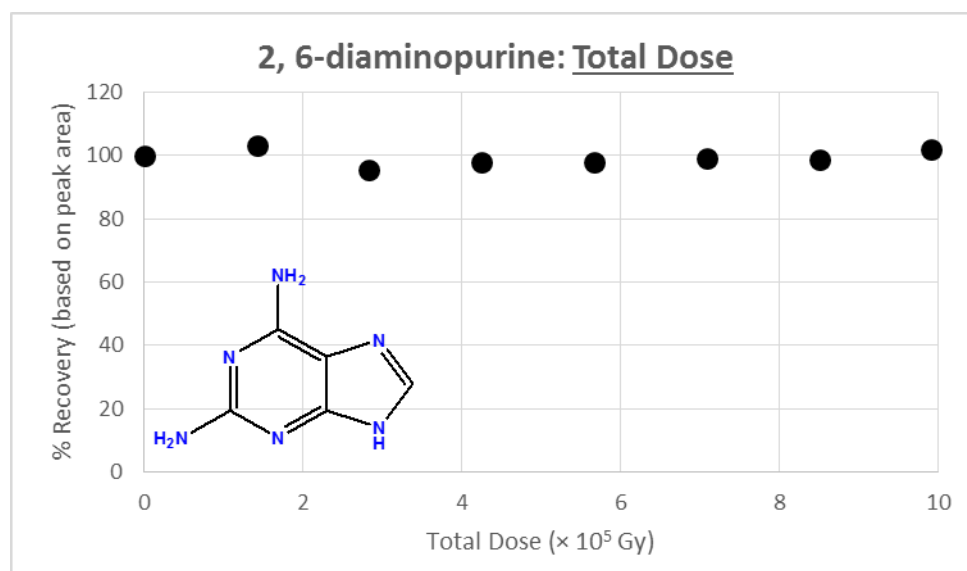


Figure 3.15. Total dose decay curve for 2,6-diaminopurine. Addition of an amine group to the 2-position does not have an effect on the stability of purine nitrogen heterocycles. 2,6-diaminopurine is considered as equally stable to γ -radiation as adenine.

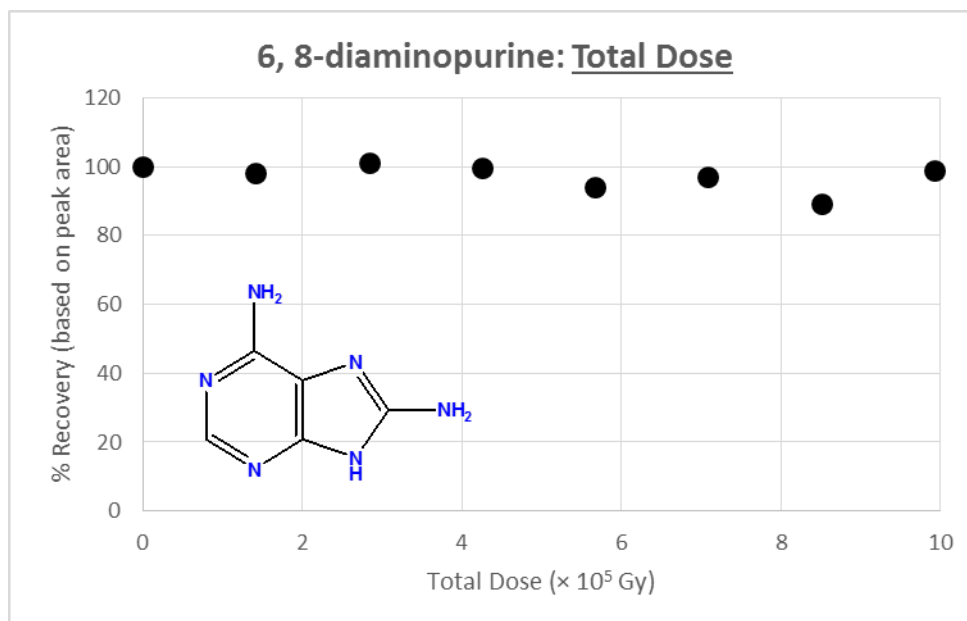


Figure 3.16. Total dose decay curve for 6,8-diaminopurine. Similar to 2,6-diaminopurine, addition of an amine group at the 8-position does not have an effect on radiolytic stability.

Table 3.3. Percent recovery of γ -irradiated nitrogen heterocycles in the total dose study. Dose rate was held constant at ~ 350 Gy/hr.

Total Dose Results for Gamma Irradiated Purines							
Dose (kGy)	Percent Content Dose Rate 350 Gy/Hr.						
	Purine	Adenine	Hypoxanthine	Guanine	Xanthine	2, 6-diaminopurine	6, 8-diaminopurine
142	97.7	102	99.6	108	98.6	103	98.3
283	93.1	102	96.7	91.1	94.5	95.4	101
425	93.5	102	98.2	88.8	94.5	98	99.6
567	93.4	95.7	98	86.7	99.2	97.9	94.3
709	95.7	97.1	95.8	83.6	99.4	99.1	97.1
850	94.2	95.5	100	76.1	96.7	98.6	89.3
992	80.1	102	103	46.8	69.5	102	99.1

Figures 3.17 shows four purine nitrogen heterocycles with amine groups in different positions and the respective decay curves for these compounds. Purine (upper left) displays nearly a 20 % decrease over the course of 1 MGy exposure. In contrast, adenine, which has an added amine group at the 6-position (upper right), is stable over the total dose range with no discernable decomposition. This same trend is observed for 2,6-

diaminopurine and 6,8-diaminopurine (lower left and lower right respectively), which both have an amine group in the same 6-position as adenine with additional amino groups on the purine ring. These purines with amine groups display what appears to be an increase in radiolytic stability and may be resistant to γ -irradiative decomposition, although further experimentation is needed in order to better define radiolytic behavior of these compounds.

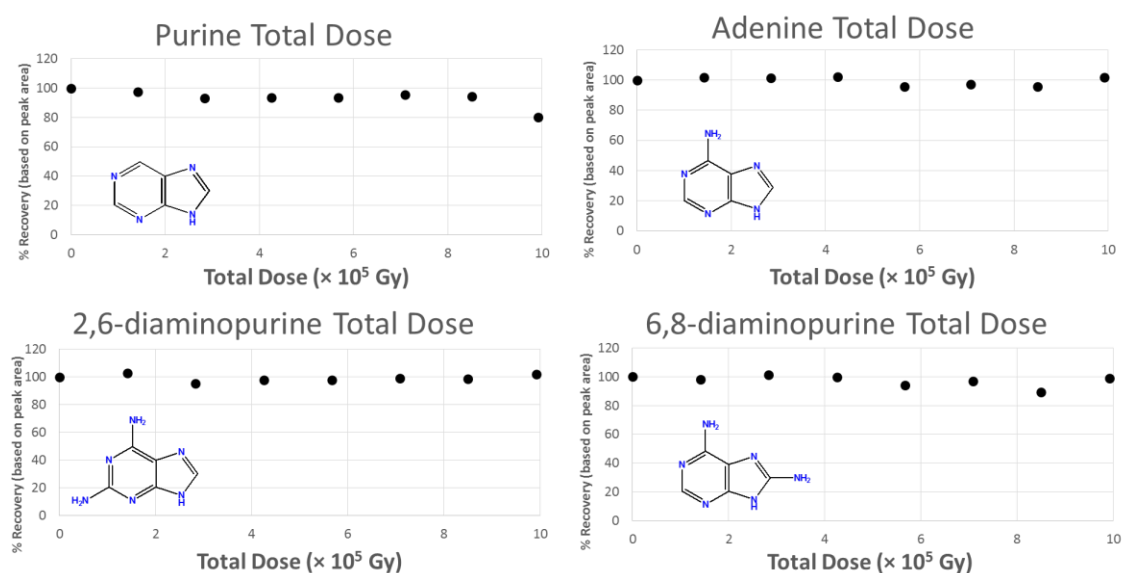


Figure 3.17. Amine substitution effects on the γ -radiolysis of purine heterocycles. The position of amine substitution appears to have a stabilizing effect on purine nitrogen heterocycles. Any noticeable decomposition (purine upper-left) occurs at total doses higher than 800 kGy.

Figures 3.18 shows decay data for adenine and guanine with their respective deamination products (replacement of an amino group with a carbonyl group), hypoxanthine and xanthine. The decay curves are shown for each of these compounds. Adenine and hypoxanthine appear to be resistant to γ -irradiation, which suggests that purines substituted at the 6-position are relatively stable. Guanine displays a decomposition of nearly 53% with exposures up to 1 MGy. Therefore, it appears that the addition of an amino group at the 2-position in combination with carbonyl substitution at the 6-position

correlates with increased radiolytic decomposition. For xanthine, the replacement of the amine at the 2-position with another carbonyl group yields some degree of stability; however, a loss of 29% over the course of 1 MGy exposure still occurs.

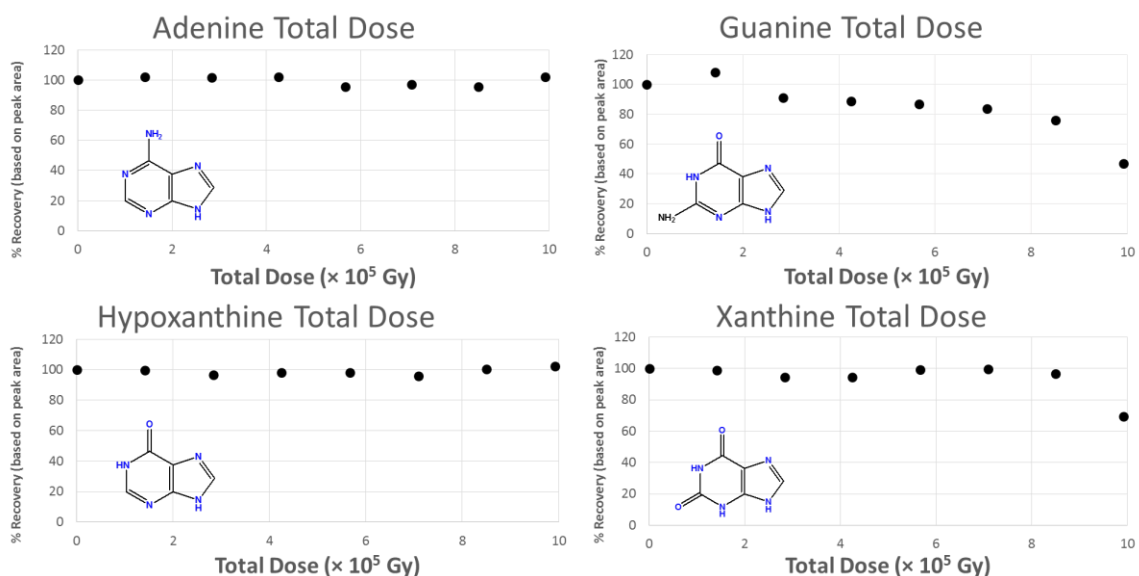


Figure 3.18. De-amination effect on the γ -radiolysis of purine heterocycles. Adenine and hypoxanthine display the same radiolytic stability while xanthine appears to be stable up to doses as high as 800 kGy, compared to guanine.

The second study performed was a dose rate analysis on the canonical purine nucleobases. The percent of irradiated nucleobase recovered was compared to an increasing dose rate (up to 350 Gy/hr) while the total dose remained constant (~ 250 kGy) to investigate the nature of irradiation products as controlled by both dose and dose rate (see **Table 3.4**). No degradation products were detected in UV chromatograms at 260 nm (or in the full spectrum scan from 200-400 nm).

The plots in **Figure 3.19** show the percent recovery (based on integrated peak area) vs. dose rate (Gy/hr). Adenine displays what could be the makings of a hyperbolic curve with an asymptote at nearly 100 % recovery. From a statistical standpoint, the lower recovery of adenine at a dose rate of ~ 87 Gy/h is calculated as an outlier at 95% confidence

using a Dixon's Q-test; however, it cannot be completely ruled out that a lower dose rate does not have an effect on adenine. On the other hand, guanine is a different story. The effect of dose rate on the nature of irradiation products is readily apparent as the percent recovery of guanine depends on both dose rate and total dose. Further investigation is warranted since these are only two examples; however, the results suggest that both parameters should be examined with each particular compound for a full understanding of its radiation chemistry.

Table 3.4. Percent recovery of γ -irradiated canonical purines in the dose rate study. The total dose received was ~ 250 kGy. The boxed X indicates that this sample was not performed for this study.

Dose Rate Results for the Canonical Purines		
Dose Rate	Percent Recovery	
(Gy/hr)	Adenine	Guanine
304	X	82
207	97.5	71
154	98.6	79.8
123	97.9	83.9
103	97	85.2
87	90.7	98

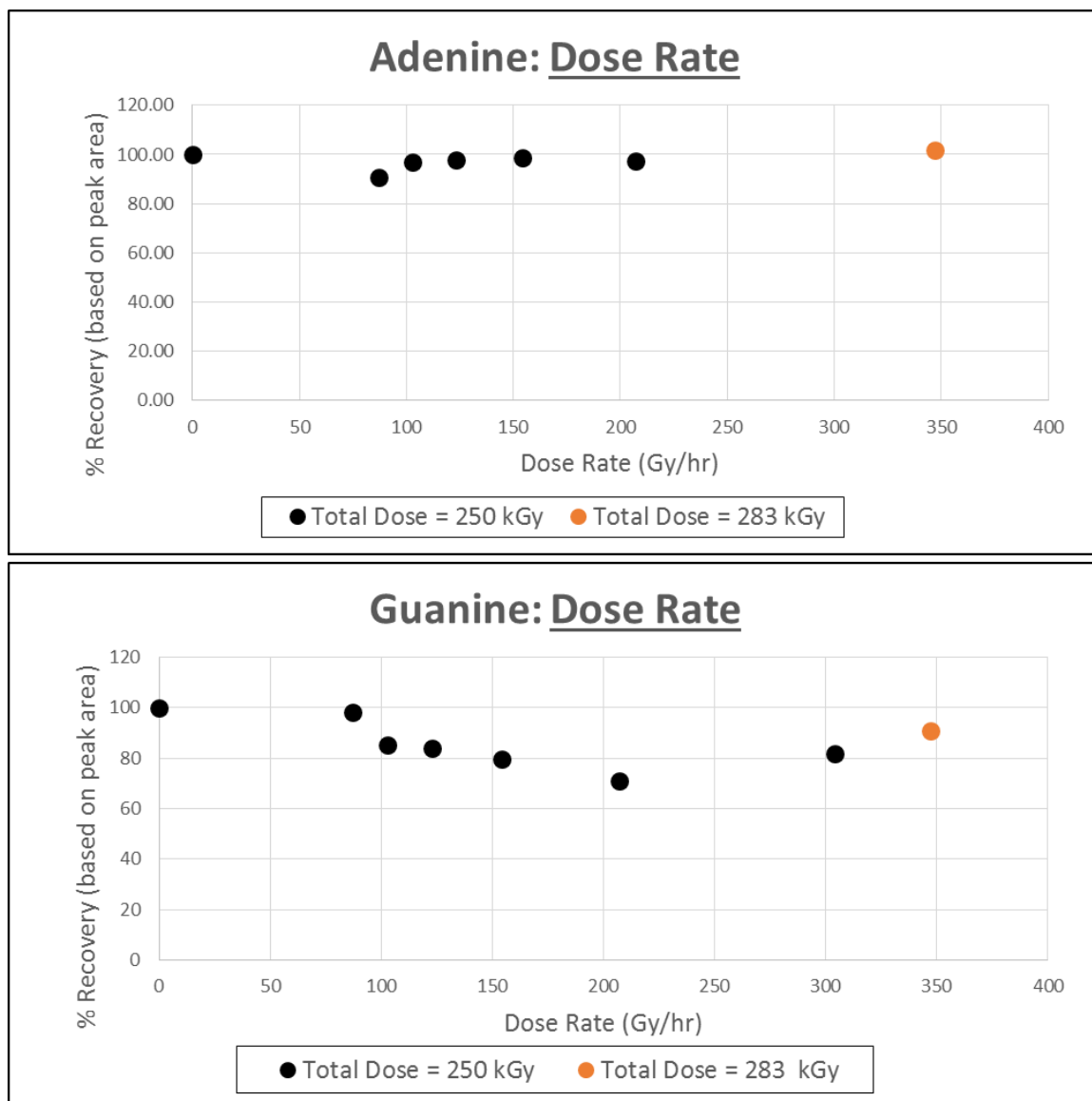


Figure 3.19. Dose rate analysis of purine nucleobases. Adenine shows stability to dose rate. However, it is not 100 % certain the datum at 87 Gy/hr is a statistical outlier. Guanine displays a strong decomposition correlating to the experienced dose rate.

Conclusion

Three trends can be inferred from the data gathered in the analysis of the γ -irradiation of purine nitrogen heterocycles. First, purine nitrogen heterocycles in the solid state irradiated by a ^{60}Co source display remarkable stability up to and including 1 MGy of total γ -irradiation dose, which is the dose equivalent to that derived by radionuclide decay

in asteroids in ~350 million years (assuming a total radiation dose of 14 MGy as calculated by Urey).^{41, 42} Second, the substitution of the purine ring structure by either amine or carbonyl groups may also have an effect on the decomposition of purine nitrogen heterocycles. Either the absence of substitution on the ring or the presence of both a carbonyl and an amine in the 2- and 6-positions may induce a state of radiolytic susceptibility. Finally, dose rate seems to have a variable effect, which might also depend on the compound being irradiated.

These results suggest that purine nucleobases and related nitrogen heterocycles are relatively stable to γ -radiation if they exist in the solid state (like in asteroids after their initial aqueous alteration period). Given this stability, one may postulate a likelihood for exogenous delivery to seed a primordial world.

REFERENCES

1. Bouvier, A.; Wadhwa, M., The Age of the Solar System Redefined by the Oldest Pb-Pb Age of a Meteoritic Inclusion. *Nature Geoscience* **2010**, *3* (9), 637-641.
2. Bachiller, R.; Forveille, T.; Huggins, P. J.; Cox, P., The Chemical Evolution of Planetary Nebulae. *Astronomy & Astrophysics* **1997**, *324* (3), 1123-1134.
3. Boger, G. I.; Sternberg, A., CN and HCN in Dense Interstellar Clouds. *Astrophysical Journal* **2005**, *632* (1), 302-315.
4. Borquez, E.; Cleaves, H.; Lazcano, A.; Miller, S., An Investigation of Prebiotic Purine Synthesis from the Hydrolysis of HCN Polymers. *Origins of Life and Evolution of Biospheres* **2005**, *35*, 79-90.
5. Burton, A. S.; Elsila, J. E.; Callahan, M. P.; Martin, M. G.; Glavin, D. P.; Johnson, N. M.; Dworkin, J. P., A Propensity for n- ω -Amino Acids in Thermally Altered Antarctic Meteorites. *Meteoritics & Planetary Science* **2012**, *47* (3), 374-386.
6. Andersen, J. L.; Andersen, T.; Flamm, C.; Hanczyc, M. M.; Merkle, D.; Stadler, P. F., Navigating the Chemical Space of HCN Polymerization and Hydrolysis: Guiding Graph Grammars by Mass Spectrometry Data. *Entropy* **2013**, *15* (10), 4066-4083.
7. Matthews, C.; Minard, R., Hydrogen Cyanide Polymers, Comets and the Origin of Life. *Faraday Discussions* **2006**, *133*, 393-401.
8. Mamajanov, I.; Herzfeld, J., HCN Polymers Characterized by SSNMR: Solid State Reaction of Crystalline Tetramer (Diaminomaleonitrile). *Journal of Chemical Physics* **2009**, *130* (13).
9. Pizzarello, S.; Williams, L.; Lehman, J.; Hollanda, G.; Yarger, J., Abundant Ammonia in Primitive Asteroids and the Case for a Possible Exobiology. *Proceedings of the National Academy of Sciences* **2011**, *108* (11), 4303-4306.
10. Minard, R.; Matthews, C., Hydrogen Cyanide Polymers Connect Cosmochemistry and Biochemistry. *Astrobiology* **2007**, *7* (3), 490-490.
11. Urey, H. C., On the Early Chemical History of the Earth and the Origin of Life. *Proceedings of the National Academy of Sciences* **1952**, *38* (4), 351-363.

12. Bernal, J. D., The Physical Basis of Life. *Proceedings of the Physical Society of London Section A* **1949**, 62 (357), 537-558.
13. Oparin, A. I., *The Origin Of Life*. Macmillan: New York, 1938.
14. Miller, S. L., The Mechanism of Synthesis of Amino Acids by Electric Discharges. *Biochimica et Biophysica Acta* **1957**, 23 (3), 480-489.
15. Oro, J.; Kimball, A.; Fritz, R.; Master, F., Amino Acid Synthesis from Formaldehyde and Hydroxylamine. *Archives of Biochemistry and Biophysics* **1959**, 85 (1), 115-130.
16. Oro, J., Synthesis of Adenine from Ammonium Cyanide. *Biochemical and Biophysical Research Communications* **1960**, 2 (6), 407-412.
17. Wakamatsu, H.; Yamada, Y.; Saito, T.; Kumashiro, I.; Takenishi, T., Synthesis of Adenine by Oligomerization of Hydrogen Cyanide. *Journal of Organic Chemistry* **1966**, 31 (6), 2035-+.
18. Menor-Salvan, C.; Marin-Yaseli, M. R., Prebiotic Chemistry in Eutectic Solutions at the Water-Ice Matrix. *Chemical Society Reviews* **2012**, 41 (16), 5404-5415.
19. Miller, S.; Cleaves, H., Prebiotic Chemistry on the Primitive Earth. In *Systems Biology: Genomics*, Rigoutsos, I.; Stephanopoulos, G., Eds. Oxford University Press: New York, 2007; Vol. 1, Pp 4-56.
20. Miyakawa, S.; Cleaves, H.; Miller, S., The Cold Origin of Life: B. Implications Based on Pyrimidines and Purines Produced from Frozen Ammonium Cyanide Solutions. *Origins of Life and Evolution of The Biosphere* **2002**, 32, 209-218.
21. Mamajanov, I.; Herzfeld, J., HCN Polymers Characterized by Solid State NMR: Chains and Sheets Formed in the Neat Liquid. *Journal of Chemical Physics* **2009**, 130 (13).
22. Volker, T., Polymeric Hydrocyanic Acid. *Angewandte Chemie-International Edition* **1960**, 72 (11), 379-384.
23. Matthews, C. In *Organic Matter In Space: Proceedings of the 251st IAU Symposium*, International Astronomical Union, Hong Kong, China, Cambridge University Press: Hong Kong, China, **2008**.
24. Callahan, M.; Smith, K.; Cleaves II, H.; Ruzicka, J.; Stern, J.; Glavin, D.; House, C.; Dworkin, J., Carbonaceous Meteorites Contain a Wide Range of Extraterrestrial Nucleobases. *Proceedings of the National Academy of Sciences* **2011**, 108 (34), 13995-13998.

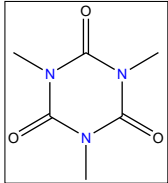
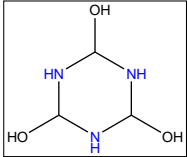
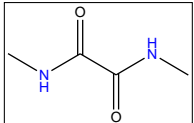
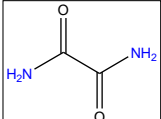
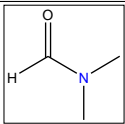
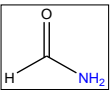
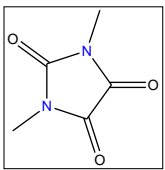
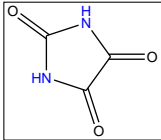
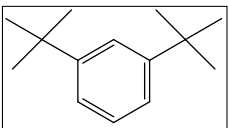

25. Hsieh, H. H.; Jewitt, D., A Population of Comets in the Main Asteroid Belt. *Science* **2006**, *312* (5773), 561-563.
26. Jewitt, D.; Luu, J., Discovery of the Candidate Kuiper Belt Object 1992 QB(1). *Nature* **1993**, *362* (6422), 730-732.
27. Oort, J. H., The Structure of the Cloud of Comets Surrounding the Solar System, and a Hypothesis Concerning Its Origin. *Bulletin of the Astronomical Institutes of the Netherlands* **1950**, *11* (408), 91-110.
28. Spratt, C. E., The Hungaria Group of Minor Planets. *Journal of the Royal Astronomical Society of Canada* **1990**, *84* (2), 123-131.
29. Pierens, A.; Raymond, S. N.; Nesvorniy, D.; Morbidelli, A., Outward Migration of Jupiter and Saturn in 3:2 or 2:1 Resonance in Radiative Disks: Implications for the Grand Tack and Nice Models. *Astrophysical Journal Letters* **2014**, *795* (1), 6.
30. Sephton, M., Organic Compounds in Carbonaceous Meteorites. *Natural Product Reports* **2002**, *19*, 292-311.
31. Todd, R. T., *Meteorites: a Chemical and Petrological Synthesis*. Cambridge University Press: Cambridge, 1981.
32. Gomes, R.; Levison, H.; Tsiganis, K.; Morbidelli, A., Origin of the Cataclysmic Late Heavy Bombardment Period of the Terrestrial Planets. *Nature* **2005**, *435*, 466-469.
33. Laufer, D.; Notesco, G.; Bar-Nun, A., From the Interstellar Medium to Earth's Oceans Via Comets - an Isotopic Study of HDO/H₂O. *Icarus* **1999**, *140* (2), 446-450.
34. Burton, A.; Stern, J.; Elsila, J.; Glavin, D.; Dworkin, J., Understanding Prebiotic Chemistry Through the Analysis of Extraterrestrial Amino-Acids and Nucleobases in Meteorites. *Chemical Society Reviews* **2012**, *41*, 5459-5472.
35. Shimoyama, A.; Hagishita, S.; Harada, K., Search for Nucleic-Acid Bases in Carbonaceous Chondrites from Antarctica. *Geochemical Journal* **1990**, *24* (5), 343-348.
36. Scott, E., Meteorite Evidence for the Accretion and Collisional Evolution of Asteroids. In *Asteroids III*, Bottke Jr, W.; Cellino, A.; Paolicchi, P.; Binzel, R., Eds. The University of Arizona Press and Lunar and Planetary Institute: Tucson, AZ, USA, 2002; Pp 697-709.
37. Huss, G.; Rubin, A.; Grossman, J., Thermal Metamorphism in Chondrites. *Meteorites in the Early Solar System II* **2006**, *943*, 567-586.
38. Draganic, I. G.; Draganic, Z. D.; Adloff, J. P., *Radiation and Radioactivity on Earth and Beyond*. Second Ed.; CRC Press: Boca Raton, FL, 1993.

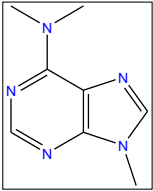
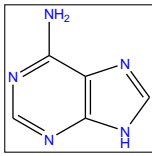
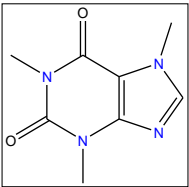
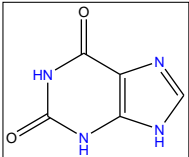
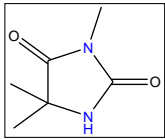
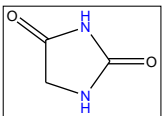
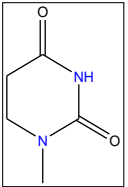
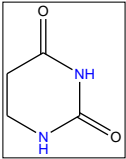
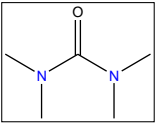
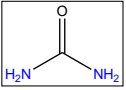
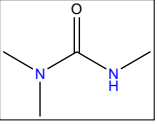
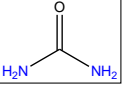
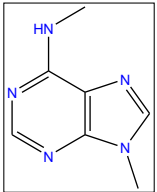
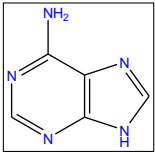
39. Garenne, A.; Beck, P.; Montes-Hernandez, G.; Brissaud, O.; Schmitt, B.; Quirico, E.; Bonal, L.; Beck, C.; Howard, K. T., Bidirectional Reflectance Spectroscopy of Carbonaceous Chondrites: Implications for Water Quantification and Primary Composition. *Icarus* **2016**, *264*, 172-183.
40. De La Fuente, J.; Ruiz-Bermejo, M.; Menor-Salván, C.; Osuna-Esteban, S., Thermal Characterization of HCN Polymers by TG-MS, TG, DTA and DSC Methods. *Polymer Degradation and Stability* **2011**, *96*, 943-948.
41. Urey, H. C., The Cosmic Abundances of Potassium, Uranium, and Thorium and the Heat Balances of the Earth, the Moon, and Mars. *Proceedings of the National Academy of Sciences* **1955**, *41* (3), 127-144.
42. Urey, H. C., The Cosmic Abundances of Potassium, Uranium, and Thorium and the Heat Balances of the Earth, the Moon, and Mars. *Proceedings of the National Academy of Sciences* **1956**, *42* (12), 889-891.
43. Khare, B.; Sagan, C.; Thompson, W.; Arakawa, E.; Meisse, C.; Tuminello, P., Optical Properties of Poly-HCN and their Astronomical Applications. *Canadian Journal of Chemistry* **1994**, *72*, 678-694.
44. De La Fuente, J.; Ruiz-Bermijo, M.; Nna-Mvondo, D.; Minard, R., Further Progress into the Thermal Characterization of HCN Polymers. *Polymer Degradation and Stability* **2014**, *110*, 241-251.
45. Mutsukura, N.; Akita, K., Infrared Absorption Spectroscopy Measurements of Amorphous CN_x Films Prepared in CH₄/N₂ R.F. Discharge. *Thin Solid Films* **1999**, *349* (1-2), 115-119.
46. Liebman, S.; Pesce-Rodriguez, R.; Matthews, C., Organic Analysis of Hydrogen Cyanide Polymers: Prebiotic and Extraterrestrial Chemistry. *Advances in Space Research* **1995**, *15* (3), 371-380.
47. Menor-Salvan, C.; Ruiz-Bermejo, D. M.; Guzman, M. I.; Osuna-Esteban, S.; Veintemillas-Verdaguer, S., Synthesis of Pyrimidines and Triazines in Ice: Implications for the Prebiotic Chemistry of Nucleobases. *Chemistry-a European Journal* **2009**, *15* (17), 4411-4418.
48. Schmitt-Kopplin, P.; Gabelica, Z.; Gougeon, R. D.; Fekete, A.; Kanawati, B.; Harir, M.; Gebefuegi, I.; Eckel, G.; Hertkorn, N., High Molecular Diversity of Extraterrestrial Organic Matter in Murchison Meteorite Revealed 40 Years After its Fall. *Proceedings of the National Academy of Sciences* **2010**, *107* (7), 2763-2768.

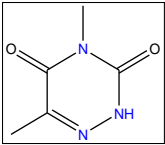
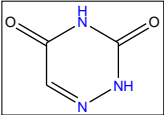
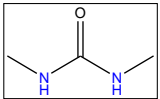
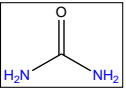
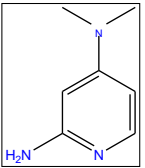
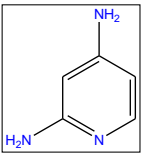
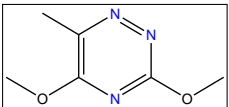
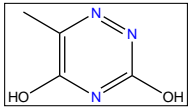
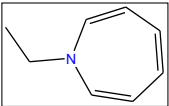
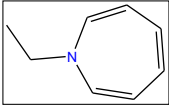
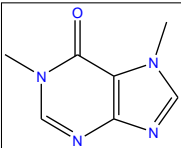
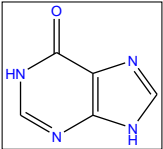
49. Draganic, I.; Draganic, Z.; Shimoyama, A.; Ponnampereuma, C., Evidence of Amino-acids in Hydrolysates of Compounds Formed by Ionizing-radiations .2. Aqueous-Solutions of CH₃CN and C₂H₅CN. *Origins of Life and Evolution of the Biosphere* **1977**, 8 (4), 377-382.
50. Kohman, T. P., Aluminum-26: A Nuclide For All Seasons (Vol 219, Pg 165, 1997). *Journal of Radioanalytical and Nuclear Chemistry* **1997**, 224 (1-2), 177-177.
51. Kohman, T. P., Aluminum-26: A Nuclide For All Seasons. *Journal of Radioanalytical and Nuclear Chemistry* **1997**, 219 (2), 165-176.
52. Laboratory, K. A. P., *Nuclides and Isotopes Chart of the Nuclides*. Seventeenth Ed.; Bechtel Marine Propulsion Corporation: United States Of America, 2009.
53. Anders, E.; Grevesse, N., Abundances of the Elements - Meteoritic and Solar. *Geochimica et Cosmochimica Acta* **1989**, 53 (1), 197-214.
54. Cherubini, C.; Ursini, O., Amino Acids Chemical Stability Submitted to Solid State Irradiation: The Case Study of Leucine, Isoleucine and Valine. *Springerplus* **2015**, 4, 10.
55. Kobayashi, K.; Kaneko, T.; Saito, T.; Oshima, T., Amino Acid Formation in Gas Mixtures by High Energy Particle Irradiation. *Origins of Life and Evolution of the Biosphere* **1998**, 28 (2), 155-165.
56. Draganic, Z.; Draganic, I.; Shimoyama, A.; Ponnampereuma, C., Evidence for Amino-acids in Hydrolysates of Compounds Formed by Ionizing-radiations .1. Aqueous-Solutions of HCN, NH₄CN, And NaCN. *Origins of Life and Evolution of the Biosphere* **1977**, 8 (4), 371-376.
57. Kminek, G.; Bada, J. L., The Effect of Ionizing Radiation on the Preservation of Amino Acids on Mars. *Earth and Planetary Science Letters* **2006**, 245 (1-2), 1-5.
58. Xu, G. Z.; Chance, M. R., Radiolytic Modification and Reactivity of Amino Acid Residues Serving as Structural Probes for Protein Footprinting. *Analytical Chemistry* **2005**, 77 (14), 4549-4555.
59. Cronin, J. R.; Pizzarello, S., Amino Acid Enantiomer Excesses in Meteorites: Origin and Significance. *Life Sciences: Exobiology* **1999**, 23 (2), 293-299.
60. Marciniak, B.; Stawny, M.; Olszewski, K.; Kozak, M.; Naskrent, M., Analytical Study on Irradiated Methylxanthine Derivatives. *Journal of Thermal Analysis and Calorimetry* **2013**, 111 (3), 2165-2170.

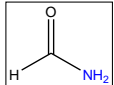
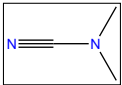
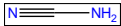
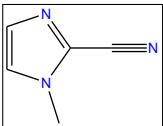
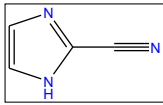
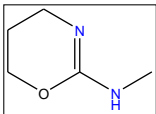
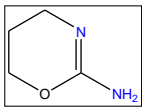
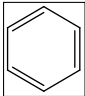
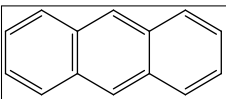
APPENDIX A

Table A.1. Compound names and structures for the products identified in the thermochemolysis TMAH-GC-MS analysis.

Compound Name and Structure of Products Identified by TMAH-GC-MS		
Compound Name	Structure	Non-derivatized Structure
cyanuric acid, trimethyl-		
N,N'-dimethyloxamide		
N,N-dimethylformamide		
1,3-dimethyl-2,4,5-trioximidazolidine		
benzene, 1,3-bis(1,1-dimethylethyl)- (a.k.a. m-di-tert-butylbenzene)		
aminoacetonitrile		

Compound Name and Structure of Products Identified by TMAH-GC-MS		
N6,N6',N9-trimethyladenine		
1,3,7-trimethylxanthine (caffeine)		
2,4-imidazolidinedione, 3,5,5-trimethyl		
1-methyl-dihydrouracil		
urea, tetramethyl-		
trimethylurea		
N6,N9-dimethyladenine		

Compound Name and Structure of Products Identified by TMAH-GC-MS		
4,6-dimethyl-3,5-dioxo-2,3,4,5-tetrahydro-1,2,4-triazine		
N,N-dimethylurea		
4-dimethylaminopyridin-2-amine		
6-azathymine, bis(methyl) ether ethylenediamine, N,N'-diethyl-N,N'-dimethyl- 6-azathymine, bis(methyl) ether		
N-ethyl-hexahydro-1H-azepine		
1,7-dimethyl-hypoxanthine		

Compound Name and Structure of Products Identified by TMAH-GC-MS		
Formamide		
Cyanamide, dimethyl		
1-methyl-1H-imidazole-2-carbonitrile		
2-methyliminoperhydro-1,3-oxazine		
benzene		
anthracene		
phenanthrene	